Drell-Yan Measurements of Nucleon and Nuclear Structure with the Fermilab Main Injector: E906

J. Arrington, D. F. Geesaman (Co-Spokesperson), K. Hafidi, R. J. Holt, H. E. Jackson, D. H. Potterveld, P. E. Reimer (Co-Spokesperson), and P. Solvignon

Argonne National Laboratory, Argonne IL 60439

C. N. Brown

Fermi National Accelerator Laboratory, Batavia, IL 60510

C. A. Gagliardi and R. E. Tribble

Texas A & M University,College Station, TX 77843-3366

G. T. Garvey, M. J. Leitch, P. L. McGaughey, and J. M. Moss

Los Alamos National Laboratory, Los Alamos, NM 87545

D. Gaskell

Thomas Jefferson National Accelerator Facility, Newport News, VA 23606

R. Gilman, C. Glashausser, X. Jiang, E. Kuchina, R. Ransome, and E. Schulte

Rutgers University, Rutgers, NJ 08544

L. D. Isenhower, M. E. Sadler, and R. S. Towell

Abilene Christian University, Abilene, TX 79699

E. Kinney

University of Colorado, Boulder, CO 80309-0390

D. D. Koetke and J. Webb

Valparaiso University, Valparaiso, IN 46383

N. C. R. Makins and J.-C. Peng

University of Illinois, Urbana, IL 61081

(Dated: September 29, 2006)

Contents

1. INTRODUCTION

While proton structure functions have been measured with deep inelastic scattering over five orders of magnitude in both the fractional momentum of the parton, x, and the virtuality of the incident photon, Q^2, the factorizable, non-perturbative parton distributions must be determined by phenomenological fits [1–4]. Perturbative Quantum Chromodynamics (QCD) quantitatively describes the Q^2 evolution of the parton distributions, but the origins of the parton distributions themselves have not proved amenable to QCD treatment, although many *models* exist in the literature. Measurements of those distributions that are poorly determined provide vital information on nucleon structure which is used to constrain and refine the phenomenology.

Each time new data have tested underlying assumptions of the phenomenology, the phenomenology has been found wanting. For example, no known symmetry requires the equality of the anti-down $[\bar{d}_p(x)]$ and anti-up $[\bar{u}_p(x)]^1$ quark distributions in the proton, but until 1991, this was a common assumption. The first evidence to the contrary was the NMC observation [5, 6] that the integral of $\bar{d}(x) - \bar{u}(x)$ is non-zero. NA51 [7] used the Drell-Yan process to confirm the inequality of $\bar{d}(x)$ and $\bar{u}(x)$. Fermilab E866/NuSea [8–10] measured the x dependence of $\bar{d}(x)/\bar{u}(x)$ and $\bar{d}(x) - \bar{u}(x)$ from $0.015 < x < 0.35$. When these data were included in the CTEQ5 [11] and MRST [12] global fits, the sea and valence distributions changed substantially from previous parameterizations, as shown in Fig. 1. Fermilab E866/NuSea observed a striking asymmetry in the sea distributions at moderate x; however, as x increased, the sea appeared to become more flavor symmetric—a sign of a possible change in the mechanism generating the sea. At the same time, however, the statistical uncertainty of the data grew significantly.

In order to study $\bar{d}(x)/\bar{u}(x)$ at larger x and to answer a number of interesting questions relating to the parton structure of nuclei and the nucleus at higher x, the Fermilab E906 collaboration plans to make precise measurements of proton-induced Drell-Yan cross sections on hydrogen, deuterium and heavy nuclear targets using the Fermilab Main Injector as a proton source. The lower beam momentum of the Main Injector (120 GeV) provides an excellent opportunity to study these distributions at larger x. For fixed x, the Drell-Yan cross section is inversely proportional to the square of the center-of-mass energy, s. At the same time, the primary background, J/ψ produc-

---

[1] The subscript p is used to denote the proton's parton distributions (as opposed to n for the neutron). From here on, unless otherwise needed for clarity, $\bar{d}(x)$ and $\bar{u}(x)$ will refer to the distributions in the proton and the subscript p will be omitted.
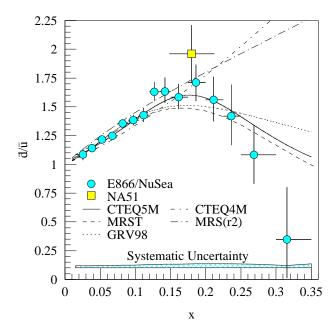
FIG. 1: FNAL E866 results [10] for the x-dependence of the ratio $\bar{d}(x)/\bar{u}(x)$ of the proton at a mass scale of 7.35 GeV. The square point is the NA51 result ($Q = 5.2$ GeV) [7]. Also shown are parameterizations of this ratio from CTEQ4M [13] and MRS(r2) [14] prior to the FNAL E866 results and parameterizations from CTEQ5M [11], MRST [12] and GRV98 [4] which have included the E866 data in the fitting procedure.

tion, which limited the instantaneous luminosity in previous experiment, scales with s and hence is reduced, allowing a more intense proton beam to be used. The combination of these yield a factor of 50 increase in the number of Drell-Yan events for the same amount of beam time. From these measurements the ratio $\bar{d}(x)/\bar{u}(x)$ for $0.1 < x < 0.45$ will be determined.

The results of these measurements will also have implications in other areas. For example, in proton-proton collider experiments the highest energy scales are achieved via $q\bar{q}$ annihilation of large x partons. Also, the observed ratio of $\bar{d}(x)/\bar{u}(x)$ results from a competition between non-perturbative and perturbative QCD gluon splitting contributions. The large x results may provide constraints on the gluon distribution that evolve into the antiquark distributions needed at high mass scales.

The absolute Drell-Yan cross sections on hydrogen and deuterium are also of great interest. In the proton, existing data allow for considerable freedom in the $d(x)/u(x)$ *quark* ratio as $x \rightarrow 1$. Through the *beam*[2] parton distributions, the proton-proton Drell-Yan cross sec-

---

[2] The subscripts 1 and 2 will be used to denote beam and target variables respectively

tion probes the linear combination $4u(x_1)\bar{u}(x_2) + d(x_1)\bar{d}(x_2)$, while proton-deuterium probes $[4u(x_1) + d(x_1)] [\bar{u}(x_2) + \bar{d}(x_2)]$ of the beam proton. The uncertainty in the parton distributions at high-x arises from a poor understanding of nuclear corrections necessary to interpret nuclear targets (even deuterium) and a lack of proton data. The absolute *proton-proton* Drell-Yan data from this experiment will be free from these uncertainties and will be able to access values of x up to 0.85. In the intermediate-x ($0.1 < x < 0.45$) deuterium absolute cross section data will provide a direct measurement of $\bar{d}(x) + \bar{u}(x)$, a quantity which was previously only measured through neutrino DIS on heavy nuclei. The interpretation of the νDIS data in terms of $\bar{d}(x) + \bar{u}(x)$, however, suffers from a lack of information on both the weak-interaction EMC effect and the difference between the valence and sea-quark EMC effect.

Additionally, proton-induced Drell-Yan cross sections on nuclear targets will be measured. These data will cleanly explore the sea-quark EMC effect. Many models of nuclear binding expect an increase in the antiquark distributions in a nucleus (for more details, see Ref. [15]). This increase has not, as yet, been observed. With better coverage at high x, E906 will be able to significantly constrain these models. Measurements of the absolute Drell-Yan cross sections on nuclei will be able to provide a direct comparison between the neutrino and the Drell-Yan deuterium data and determine how nuclear effects might influence the interpretation of the neutrino determination of $\bar{d}(x) + \bar{u}(x)$.

The data from nuclear targets will also be used to determine the energy loss of a quark traveling through a cold nucleus. The initial state beam quark will interact strongly and loose energy as it penetrates the nucleus before annihilating. The energy loss results in an apparent shift in the observed parton momentum fraction, x of the interacting quark. By comparing measurements on differently sized nuclei, the energy loss can be determined. Previous Drell-Yan experiments have placed limits on the energy loss [16], but with the higher statistics and increased sensitivity from the lower beam energy, this experiment will be able to quantitatively distinguish between competing models.

To study these issues, the E906/Drell-Yan experiment was given Stage I approval by Fermilab in November, 2001. Because of a desire to schedule E906/Drell-Yan at the same time as other proposed fixed-target experiments, E906 was not scheduled at that time. The resolution of these issues and proton economics will be discussed in Sec. 4. Since Stage I approval, the physics case has remained strong, and this experiment is still the best way to address these issues. The entire physics program of the experiment is presented in Sec. 2. The design of the E906 experimental apparatus

relies heavily on our previous experience in Fermilab E605, E772, E789 and E866/NuSea. Much of the detector hardware already exists and was used in these previous experiments or in Fermilab E871. Because of the lower energy, however, it will be necessary to fabricate coils for a new magnet. Details of the detector are given in Sec. 3 and additional cost and scheduling information are in Sec. 4. For those already familiar with the E906/Drell-Yan physics program and spectrometer design, a summary of the changes since the original proposal are given in Appendix A.

2. MEASUREMENTS WITH THE DRELL-YAN PROCESS

In the Drell-Yan process, a virtual photon is produced through the annihilation of a quark from the beam (target) with an antiquark in the from the target (beam). The virtual photon is detected through its decay into an oppositely charged lepton pair:

$$q\bar{q} \rightarrow \gamma^* \rightarrow l^+l^-. \tag{1}$$

To lowest order this process depends on the product of quark and antiquark distributions in the beam and target:

$$\frac{d^2\sigma}{dx_1 dx_2} = \frac{4\pi\alpha^2}{9sx_1x_2} \sum_i e_i^2 \left[q_{1i}(x_1, Q^2)\bar{q}_{2i}(x_2, Q^2) + \bar{q}_{1i}(x_1, Q^2)q_{2i}(x_2, Q^2) \right]. \tag{2}$$

where q_{1i} (q_{2i}) are the beam (target) quark distributions and the sum is over all quark flavors (u, d, s, c, b, t) and e_i is the quark's charge. The fraction of the longitudinal momentum of the beam (target) carried by the participating quarks is $x_{1(2)}$. The squared total energy of the beam-target system, for a fixed target experiment, is $s = 2m_2E_1 + m_1^2 + m_2^2$ where E_1 the energy of the beam hadron and m_1 (m_2) the rest masses of the beam (target) hadron. In the case of nuclear targets, it is assumed that the reaction takes place on a component nucleon, $m_2 = M_n$, where M_n is the nucleon mass, and the momentum fraction, x_2 refers to the fractional momentum of the parton relative to the interacting nucleon.

The sensitivity of the Drell-Yan process to the antiquark distributions of the target and beam is clear from examining Eq. 2. At large values of x, the parton distributions are dominated by the valence distributions and at small x by the sea distributions. Thus, in the limit of large x_1 and small x_2, the cross section is dominated by the first term—the annihilation of *beam quarks* with *target antiquarks*— providing direct sensitivity to the antiquark sea of the target nuclei. This limit is exactly the kinematics selected by a dipole-based spectrometer's acceptance in a fixed-target environment where all particles are boosted very far forward.

E906/Drell-Yan will extend the measurements made by E866/NuSea to $x_2 \approx 0.45$. For this, beams from the 120 GeV Fermilab Main Injector have two primary advantages compared with previous 800 GeV measurements:

- For fixed x_1 and x_2 the Drell-Yan cross section is proportional to $1/E_b$, where E_b is the incident beam energy, as shown in Eq. 2. A 120 GeV Main Injector experiment will have a factor of nearly 7 times larger cross sections compared with previous experiments which used an 800 GeV extracted Tevatron beam.

- Practical limitations in the acceptable luminosity for these experiments are radiation protection limits and the single muon rates in the detectors. To the extent that the radiation dose scales as beam power, one can take approximately 7 times the luminosity for the same beam power at 120 GeV relative to 800 GeV. In E866 at 800 GeV, J/ψ events from the beam dump were a significant contribution to the muon singles rates. At 120 GeV the total J/ψ production cross sections fall by an order of magnitude when compared with 800 GeV.

The combination of these effects is expected to allow a factor of nearly 50 improvement in the number of recorded events at high x_2 when compared with previous Drell-Yan experiments.

The kinematics of the virtual photon in the Drell-Yan process—longitudinal center of mass momentum $p_\parallel^\gamma$, transverse momentum p_T^γ and mass M_γ—are determined by measuring its the two-muon decay. These quantities determine the momentum fractions of the two interacting quarks:

$$y = \frac{1}{2} \ln \left[\frac{E^\gamma + p_\parallel^\gamma}{E^\gamma - p_\parallel^\gamma} \right] \text{ and } \tau = M_\gamma^2/s. \tag{3}$$

From this,

$$x_{1,2} = \sqrt{\tau} e^{\pm y}. \tag{4}$$

In the limit of no transverse momenta, these are equivalent to

$$x_F = \frac{p_\parallel^\gamma}{p_\parallel^{\gamma,\max}} \approx x_1 - x_2 \text{ and } x_1 x_2 s = M_\gamma^2 \tag{5}$$

where $p_\parallel^{\gamma,\max}$ is the maximum kinematic value $p_\parallel^\gamma$ can have.

2.1. Parton Distributions: $\bar{d}(x)/\bar{u}(x)$ of the Proton

The ratio of $\bar{d}(x)/\bar{u}(x)$ in the proton may be determined by measuring the ratio of proton induced Drell-Yan on deuterium to that on hydrogen. Both Fermilab E866 and CERN NA51 used

this method to determine $\bar{d}(x)/\bar{u}(x)$. To extract this from the measured ratio, nuclear effects in deuterium were ignored—its cross section was treated as the sum of the free proton and free neutron cross sections and charge symmetry was then used to equate $\bar{d}_p$ to $\bar{u}_n$ and $\bar{u}_p$ to $\bar{d}_n$. To illustrate the sensitivity of Drell-Yan to this ratio, the ratio of cross sections can be expresses as

$$\left.\frac{\sigma^{pd}}{2\sigma^{pp}}\right|_{x_1 \gg x_2} \approx \frac{1}{2} \left[\frac{1 + \frac{d(x_1)}{4u(x_1)}}{1 + \frac{d(x_1)}{4u(x_1)} \frac{\bar{d}(x_2)}{\bar{u}(x_2)}} \right] \left[1 + \frac{\bar{d}(x_2)}{\bar{u}(x_2)} \right]. \tag{6}$$

after ignoring the the strange and heavier quark contribution and taking the limit that $x_1 \gg x_2$ (*i.e.* the kinematics selected by the spectrometer, implying the beam antiquark-target quark contribution is small). Then observing that $d(x) \ll 4u(x)$, this expression simplifies even further to

$$\left.\frac{\sigma^{pd}}{2\sigma^{pp}}\right|_{x_1 \gg x_2} \approx \frac{1}{2} \left[1 + \frac{\bar{d}(x_2)}{\bar{u}(x_2)} \right]. \tag{7}$$

The actual extraction of $\bar{d}(x)/\bar{u}(x)$ performed by E866/NuSea and which will be performed by E906/Drell-Yan used Eq. 2 and was verified with full next-to-leading order (NLO) cross section calculations. The $\bar{d}(x)/\bar{u}(x)$ extractions were also verified through next-to-leading order global fits to the measured cross section ratios by CTEQ [1], MRST [12] and GRV [4].

The expected statistical precision with which the ratio $\sigma^{pd}/2\sigma^{pp}$ will be measured in this experiment is shown in Fig. 2 along with the E866 measurements. It is apparent that a high luminosity Main Injector experiment can extend the x range of our knowledge of $\bar{d}(x)/\bar{u}(x)$ up to $x \approx 0.45$.

As can be seen by comparing the $\bar{d}(x)/\bar{u}(x)$ curves shown in Fig. 1, the inclusion of the E866 data completely changed the parameterization of the antiquark sea for $x > 0.20$. In determining the anti-quark content of the proton sea, the parton distribution fits have simply parameterized the E866 data with a convenient algebraic form. While the chosen form reproduces the Drell-Yan data well, the statistical uncertainty on the data still allows for up to a 50% variation at $x = 0.3$ compared with only a few percent uncertainty up to $x = 0.4$ which would be achieved by the present proposal, as shown in Fig. 2.

2.1.1. Origins of the Nucleon Sea

While providing direct input to the parton distribution fits, the ultimate impact of this experiment will be to provide a better understanding on the physical mechanism which generates the sea of the proton. The $\bar{d}(x) - \bar{u}(x)$ difference, shown in Fig. 3, is a pure flavor non-singlet quantity: its integral is Q^2 independent [17] and its Q^2 evolution at leading order does not depend on the
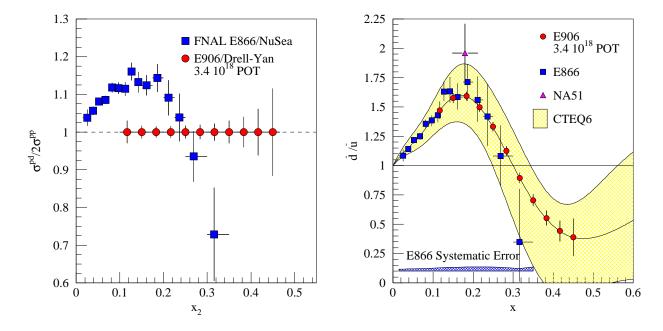
FIG. 2: FNAL E866 results[8, 10] for the ratio of $\sigma^{pd}/2\sigma^{pp}$ (left) and $\bar{d}(x)/\bar{u}(x)$ (right). The statistical uncertainties expected for the measurement proposed here are shown on the solid circles (arbitrarily plotted at 1.0 for the cross section ratio and following the CTEQ6 curve for $\bar{d}(x)/\bar{u}(x)$)). In the $\bar{d}(x)/\bar{u}(x)$ plot, the yellow band illustrates the uncertainty from the CTEQ6m fit. The systematic uncertainty for the E906/Drell-Yan $\bar{d}(x)/\bar{u}(x)$ extraction is estimated to be less than 1%.

gluon distribution of the proton. Early expectations were that Pauli blocking due to the extra valence u quark in the proton would lead to a suppression of $g \to u\bar{u}$ which would contribute significantly to differences in the light sea [18]. These expectations were not, however, borne out by calculations [19, 20] (though this point is still debated in the literature [21]). In perturbative QCD, differences between the $\bar{d}(x)$ and $\bar{u}(x)$ distributions arise only at second order and are calculated to be very small [19]. The large differences seen in Figs. 1, 2 and 3 must be non-perturbative in nature and are likely explained in terms of collective degrees of freedom of QCD at low energy.

There are three significant non-perturbative approaches that can accommodate large differences in $\bar{d}(x) - \bar{u}(x)$: (1) hadronic models of the meson cloud of the nucleon, (2) chiral quark models which couple mesons directly to constituent quarks and (3) instanton models. Figure 3 illustrates calculations for representative examples of each of these models. An intriguing feature is that in each of these models the flavor and spin distributions of the proton are intimately linked. As these non-perturbative models are considered, it is important to remember that they must be combined with perturbative sources to generate the entire quark sea of the proton.
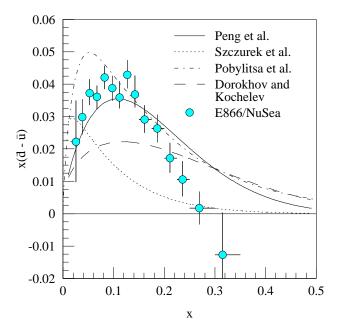
FIG. 3: Fermilab E866/NuSea results [8–10] for $x\left[\bar{d}(x) - \bar{u}(x)\right]$ at a mass scale of 7.35 GeV. The curves represent four model calculations of $x\left[\bar{d}(x) - \bar{u}(x)\right]$. The solid curve is a meson-cloud model calculation including nucleons, deltas and pions [9]. The dotted and dot-dashed curves are a chiral quark models [22, 23] and the long-dashed curve is an instanton inspired parameterization [24].

The pion cloud model has a tantalizing simplicity and does explain basic features of the data. A proton wave function containing sizable virtual $|n\pi^+\rangle$ Fock states will have an excess of $\bar{d}$-quarks from the valence quarks in the π^+. The difficulty in this approach is finding justification to truncate the hadronic expansion [25]. Most calculations include contributions for $|N\pi\rangle$ and $|\Delta\pi\rangle$ states (*e.g.* Ref. [26, 27]). The pion-nucleon and pion-delta coupling constants ($g_{\pi NN}$ and $g_{\pi N\Delta}$) are well known, so the primary difference among calculations is the treatment of the πNN and $\pi N\Delta$ vertex factors. Using "not unreasonable" vertex functions (dipole vertex functions with cut offs, Λ, of $\Lambda_{\pi NN} = 1.0$ GeV and $\Lambda_{\pi N\Delta} = 0.8$ GeV) reasonable agreement with the data [9] is found as show in the solid curve of Fig. 3. The resulting probabilities for the $|N\pi\rangle$ and $|\Delta\pi\rangle$ admixture lead to a prediction for the difference in total spin carried by the u quarks (Δu) and the d quarks (Δd), $\Delta u - \Delta d = G_A$ of approximately 1.5 [9], providing part of the reduction from the quark model value of 5/3.

Chiral field theories suggest that the relevant degrees of freedom are constituent quarks, gluons and Goldstone bosons. Processes such as $u \rightarrow d\pi^+$ and $d \rightarrow u\pi^-$ generate a flavor asymmetry in the sea simply because there are more up than down quarks in the proton. Two predictions of

$\bar{d}(x) - \bar{u}(x)$ from chiral models are shown in Fig. 3 as the dotted and dot-dashed curves. Clearly the model of Szczurek *et al.* [22] is too soft. The chiral quark-soliton model of Pobylitsa *et al.* [23] better reproduces the measured $x\left[\bar{d}(x) - \bar{u}(x)\right]$ distribution for $x > 0.08$, but overestimates the asymmetry at small x.

Instanton effective Lagrangians imply coupling at the tree level between instantons and the valence quarks which leads to a $\bar{d}(x) - \bar{u}(x)$ difference. This raises the intriguing possibility that Drell-Yan measurements could provide experimental information on these theoretically very useful but seemingly experimentally inaccessible constructs. Within the framework of the t'Hooft SU(2) effective Lagrangian [28] (which is of the form $\bar{u}_R u_L \bar{d}_R d_L + \bar{u}_L u_R \bar{d}_L d_R$ where the subscripts R and L label the quark helicity) the u quarks generate a $\bar{d}d$ sea and the helicity of the valence quarks is screened [24]. (A flavor SU(3) Lagrangian would also generate $s\bar{s}$ pairs.) Dorokhov and Kochelev [24] fit the NMC measurement of the $\bar{d}(x) - \bar{u}(x)$ integral to a form parameterized to have the expected asymptotes which is shown as the long-dashed curve on Fig. 3. The $\bar{d}(x) - \bar{u}(x)$ difference observed by E866 does not show the expected transverse momentum (p_T) dependence, however. One of prediction of instanton models is the relations between the instanton contributions (subscript I in Eq. 8) of the spin and flavor matrix elements, for example:

$$\bar{d}_I(x) - \bar{u}_I(x) = \frac{3}{5}\left[\Delta u_I(x) - \Delta d_I(x)\right] \tag{8}$$

It is interesting to note that while this approach gives a reduction in the total spin carried by the quarks in the nucleon, it implies an increase in $\Delta u_I(x) - \Delta d_I(x)$ while in the other models an increase in the flavor asymmetry causes a decrease in $\Delta u(x) - \Delta d(x)$.

As mentioned earlier, none of these models consistently incorporate the flavor symmetric sea and consequently all substantially over predict the ratio of $\bar{d}(x)/\bar{u}(x)$ for $x > 0.23$. Unfortunately the statistical uncertainty on the E866 data becomes large in this region. The pion models tend to level off at a predicted non-perturbative $\bar{d}(x)/\bar{u}(x)$ between 1.5 and 5 (depending on the baryons and mesons included in the calculations) until $x > 0.5$ where the ratio begins to decrease slowly to unity. The instanton model predicts a ratio of $\bar{d}(x)/\bar{u}(x) \approx 4$ at high x. One possible interpretation of the E886 results is that the perturbative gluon mechanism begins to establish its dominance over the non-perturbative mechanisms at a lower value of x than previously expected, indicating a larger gluon component in the proton. The gluon distribution at high x is, at present, poorly constrained, with uncertainties of 30-40% at $x = 0.4$ [1, 29].

2.1.2.   Interpretability of the Results: QCD factorization

The interpretability of Drell-Yan results as direct measures of the parton distributions is based on the QCD factorization theorems [30–32]. Bodwin, Brodsky and Lepage [32] give the condition for the minimum beam momentum $P_{\min}$ below which initial state QCD interactions become important as:

$$P_{\min} \approx \frac{p_T A^{2/3}}{x_1}. \tag{9}$$

A conservative estimate of $\langle p_T^2 \rangle \approx 0.4$ GeV^2 (Ref. [32] uses 0.25 GeV) yields a typical transverse hadronic scale p_T on the order of 0.6 GeV and a minimum beam momentum of 23 GeV for $x_1 > 0.3$ and a calcium target, comfortably below the 120 GeV considered here.

2.1.3.   Competing Measurements of $\bar{d}/\bar{u}$

We know of no significant competition for measurements of the flavor dependence of antiquark distributions in this x range. The classes of experiments with potential sensitivity are neutrino deep inelastic scattering (νDIS), semi-inclusive deep inelastic scattering (SIDIS), electroweak boson production at pp colliders and other Drell-Yan measurements. Each is considered briefly in turn.

The magnitude of the antiquark sea $\bar{d} + \bar{u} + \bar{s}$ may be determined by νDIS, and CCFR and NuTeV [33–35] have accumulated large amounts of ν and $\bar{\nu}$DIS data. However, on an isoscalar target have little sensitivity to the asymmetry of the sea, $\bar{d} - \bar{u}$. There are also uncertainties from nuclear effects in heavy targets which affect extraction of $\bar{d} + \bar{u}$ from the νDIS data. In this respect, E906/Drell-Yan data will be complimentary, with both light and heavy target data in a kinematic range overlapping the νDIS data.

The flavor dependence of the parton fragmentation functions is used in SIDIS to disentangle the contributions of the different parton distributions. The HERMES collaboration at DESY has used SIDIS to study the flavor dependence of the sea [36]. The HERMES results agree well with the E866 results but have factors of 5 larger error bars, as shown in Fig. 4. SIDIS most directly measures

$$\frac{\bar{d}(x) - \bar{u}(x)}{u(x) - d(x)} = \frac{J(z)\left[1 - r(x,z)\right] - \left[1 + r(x,z)\right]}{J(z)\left[1 - r(x,z)\right] + \left[1 + r(x,z)\right]}, \tag{10}$$

with

$$r(x,z) = \frac{N_p^{\pi^-} - N_n^{\pi^-}}{N_p^{\pi^+} - N_n^{\pi^+}}. \tag{11}$$

Here, $J(z)$ depends on the fragmentation functions and z is the fraction of the energy of the virtual photon carried by the hadron. At high x where the difference of antiquark distributions is much smaller than the difference of quark distributions, one must measure differences of several comparable size numbers. Additionally, the systematic uncertainty due to the fragmentation physics is also an issue. The experiments which can improve these measurements are HERMES and COMPASS, both of which concentrate on polarized structure function measurements. While HERMES will has increased the size of their data set significantly with high-density unpolarized running, they will not be able to extend their x range significantly to higher x, and will be limited by systematic uncertainties. The COMPASS experiment at CERN could do similar semi-inclusive SIDIS measurements. To date they have not proposed dedicated unpolarized running with rapid interchange of pure hydrogen and deuterium targets. There have been proposals for similar measurements at Jefferson Laboratory for both the current facility [37] (deferred) and the upgraded 12 GeV facility [38] (also deferred). Even if the 12 GeV proposal (in which the necessary DIS kinematics are more accessible than the 6 GeV proposal) were approved, the measurement would cover a more limited range, and then with significantly larger statistical uncertainty (on the order of 10-15% as compared with 1-4% for most of the E906/Drell-Yan data). Furthermore, the theoretical interpretation of the data in terms of $\bar{d}(x) - \bar{u}(x)$ is not as clean as for Drell-Yan, and their agreement with Drell-Yan data may be viewed as a test of factorization at these energies rather than a measurement of $\bar{d} - \bar{u}$

The production of W bosons in p-p collisions does offer sensitivity to the antiquark distributions. At the LHC one only has sensitivity for the x range considered here at the highest rapidities ($y > 4$). However at RHIC higher x values are quite relevant and plans are underway to use the W decay asymmetry in single spin asymmetries to study the antiquark polarization. Since the RHIC detectors have limited kinematic coverage and these events have missing transverse energy, the parton level kinematics of each event are not well determined and one averages over a significant x region. With the antiquark distributions falling rapidly, the lepton asymmetry yields are dominated by lower x values. We have discussed the plans with members of the STAR and PHENIX collaborations at RHIC. They concluded that they will not be sensitive to the antiquark distributions at $x > 0.2$.

In contrast to processes like SIDIS, the Drell-Yan measurement of $\bar{d}/\bar{u}$ has much smaller systematic errors and acceptance corrections. In the long term future, the lower-energy, high-intensity Japan Proton Accelerator Research Complex (J-PARC) may be able to address this physics. Eventually, it will have a 50 GeV, slow-extraction proton beam. When this facility is completed, a
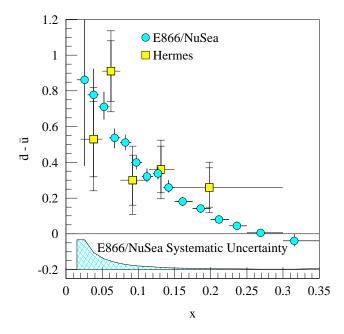
FIG. 4: Measurement of $\bar{d}(x) - \bar{u}(x)$ from HERMES [36] compared with the measurements of FNAL E866/NuSea [8, 10]. The inner error bars on the HERMES data points represent the statistical uncertainty while the outer error bars represent the statistical and systematic uncertainty added in quadrature. The uncertainty shown on the E866/NuSea data is statistical, with the common systematic uncertainty shown by the band at the bottom.

Drell-Yan experiment could be mounted. The current Phase I facility will have a 30 GeV proton beam. In Phase I, this effectively limits a di-muon experiment to studying the J/ψ. A di-muon experiment has been proposed for JPARC, focusing on J/ψ physics during the Phase I period and then Drell-Yan physics once the Phase II upgrade is completed. The JPARC PAC recognized the importance of the Drell-Yan program, but deferred this experiment citing the present lack of the 50 GeV facility and the uncertainty attaining it. Eventually, with a 50 GeV beam, lower proton beam energy at J-PARC implies that an experiment there could be sensitive to a higher range of x_{target} values (0.2–0.6) than covered by E906 (0.1–0.45). This additional reach in x_{target} has significant costs associated with it:

- The interpretability of Drell-Yan results as direct measures of parton distributions is based on QCD factorization. Using the criteria of Bodwin, Brodsky and Lepage [30–32] discussed in Sec. 2.1.2, the 50 GeV proton beam energy may be marginal for use with the nuclear targets, at least for some of the x_{beam} range.

- From an experimental point of view at 50 GeV, the background from pion decay will significantly increase because of the lower boost. *Decreasing* the target-absorber separation may partly over come this difficulty. At the same time, however, the lower energy muons will have greater multiple scattering and energy loss while traveling through the hadron absorber, making separation of muons produced in the target and in the beam dump/absorber very tricky—calling for an *increased* target-absorber distance. It may not be possible to balance these competing needs at 50 GeV.

- The x_{target} range provides very little overlap with existing Drell-Yan data (Fermilab E772 [39] or E866 [8, 10]) making consistency checks difficult, whereas it will be straightforward to cross-check E906 results with those of E772 and E866.

- After imposing a mass cut to remove the J/ψ, the limitations of a 50 GeV beam impose a *necessary* kinematic correlation between x_{beam} and x_{target}. For studies with nuclear targets, there will be no kinematic region in which either nuclear target or energy loss effects are already known to be small.

The Main Injector appears to have been fortuitously optimized the combination of reliable interpretation and attainable precision.

Experts like James Stirling [40] (of MRST) have given their strongest support to our proposal as the best way to measure the flavor dependence of the antiquark distributions at high x. Again we see no serious competition for this experiment in the near future.

2.1.4. Results and Yields

The expected statistical uncertainties and yields show in this proposal result from Monte Carlo simulations of this experiment with the proposed apparatus, outlined in Sec. 3. The statistical uncertainty is based on a total integrated incident beam of 5.2×10^{18} protons. These were divided between the targets: 35% hydrogen, 26% deuterium, 4% dummy liquid cell, 35% nuclear targets (3 targets). With this luminosity E906/Drell-Yan will achieve the relative errors on the ratio of the deuterium to hydrogen cross sections for $x_F > -0.1$ shown in Fig. 2. E866/NuSea was able to maintain systematic errors on the cross section ratio to better than 1%, and it is anticipated that E906/Drell-Yan will also be able to achieve 1% systematic errors in the ratio. With these yields, the statistical precision of the extraction of $\bar{d}/\bar{u}$ is shown in Fig. 2 relative to the expectation from
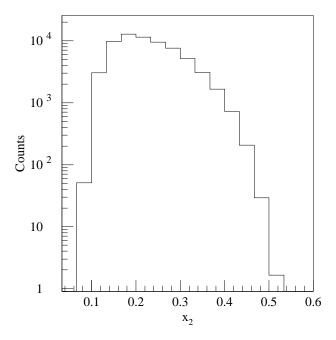
FIG. 5: Monte Carlo results for yields from 1.4×10^{18} protons on on a 50 cm long liquid deuterium target with the proposed apparatus. This represents all accepted events with masses between 4.2 and 8.5 GeV with $x_F > -0.1$

the CTEQ6m parton distributions. The integrated number of counts are shown as a function of x_2 in Fig. 5.

2.2. Measurements of Other Parton Distributions

In addition to the Drell-Yan ratio measurement, the absolute Drell-Yan proton-hydrogen and proton-deuterium cross sections will be determined. These measurements will be sensitive to the properties of the beam proton over the range $0.3 < x_1 \leq 0.85$ and of the target over the range $0.1 < x_2 < 0.45$. The deuterium absolute cross section can be used to determine the magnitude of the anti-quark sea, $\bar{d}(x) + \bar{u}(x)$. Until now, the parton distribution fits obtained sensitivity to the magnitude of the sea distribution at high x from the CCFR neutrino measurements on iron [33] and the E605 Drell-Yan measurements on Cu [41]. The extracted magnitude of $(\bar{d} + \bar{u})$ depends on differences between neutrino, anti-neutrino and electron/muon deep inelastic scattering results. The nuclear corrections, which can be different for valence and sea quarks, are a significant uncertainty in these comparisons. One of the advances of E906 will be absolute *p-p*, *p-d* and *p-A*
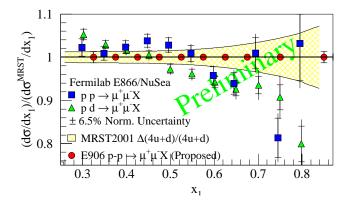
FIG. 6: The preliminary ratio of Drell-Yan cross section measured by Fermilab E866/NuSea [44] for proton-deuterium (triangles) and proton-proton (squares) to calculated NLO cross section based on the MRST2001 [29] parton distributions. The inner error bars are statistical only. The outer error bars are a *linear* sum of statistical and point-to-point systematic uncertainties. The yellow band represents the uncertainty given by MRST2001 on $4u + d$. The circles show the statistical uncertainties which will be obtained with E906, arbitrarily plotting the ratio at 1.

Drell-Yan cross sections at high x and a precise measurement of the nuclear dependence of the $\bar{d} - \bar{u}$ distribution at these x regions.

When viewed as a function of the beam momentum fraction x_1, the absolute cross section data provide information about the partonic structure of the beam proton. As $x \to 1$, the parton distributions are poorly determined. This is due to a lack of proton data and due to significant theoretical uncertainties in the interpretation of nuclear data—even in deuterium [42, 43]. Drell-Yan proton-proton data will be completely free from these uncertainties, and Drell-Yan proton-deuterium data will probe high-x of the beam proton and intermediate-x of the target deuterium, where these nuclear effects are understood. An examination of Fermilab E866/NuSea data [44] indicate that the CTEQ6 [1] and MRST2001 [29] parameterizations produce a larger NLO cross section than is actually seen at high-x as shown in Fig. 6. The E906 experiment will significantly increase the amount of data available at high-x. Fig. 6 shows the expected statistical uncertainty which will be achieved by E906.

2.3. Antiquark Distributions of Nuclei

The distributions of partons within a free nucleon differ from those of a nucleon bound within a heavy nucleus, an effect first discovered by the EMC collaboration in 1983 [45]. Much of the

data on nuclear dependencies is from charged lepton deep inelastic scattering (DIS) experiments, which are sensitive only to the charge-weighted sum of all quark and antiquark distributions. The antiquark distributions at large x are determined primarily from neutrino DIS (νDIS) on heavy targets, but there are no similar high statistics νDIS data on light (hydrogen or deuterium) targets. Nuclear effects in the sea quark distributions may be entirely different from those in the valence sector [46], and indeed, unlike electron and muon scattering, Drell-Yan data from E772 show no antishadowing, although, with limited statistical precision for $x > 0.2$ [39], as shown in Fig. 7. Higher precision data in the antishadowing region as well as at larger x than E772 could access would provide extremely valuable new information on the nuclear dependence of parton distributions. In addition, the absolute deuterium and nucleus cross section measurements will give a direct measurement of the strength of the sea ($\bar{d} + \bar{u}$) and its nuclear dependence, providing direct comparisons to neutrino-nucleus data which was previously used to determine this quantity. The expected statistical precision of the proposed measurement is shown in Fig. 8, compared with the existing Drell-Yan and DIS results on the ratios of calcium to deuterium. E906 will be able to precisely measure nuclear effects throughout the antishadowing and into the "EMC effect" region.

In the context of nuclear convolution models, virtual pion contributions to nuclear structure functions were expected to lead to sizable increases in sea distributions of the nuclei compared with deuterium. This expectation was convincingly shattered by the E772 Drell-Yan measurements [39], as shown in Fig. 7, which found little nuclear dependence except in the shadowing region. The non-observation of evidence for nuclear pions or a pion excess calls into question the most widely believed traditional meson-exchange model [47] of the nucleus, which presents a fundamental problem for nuclear physics. The expected enhancement to the sea is illustrated in Fig. 9, which shows the expected Drell-Yan ratio in iron to deuterium, based on the nuclear convolution model calculations by Coester [48–51]. More recent calculations, made in light of the E772 data, predict a smaller nuclear dependence [51–53], consistent with the statistical uncertainties of E772. Several of these calculations are discussed below, along with the estimates of the size of effect expected in a Drell-Yan experiment. Jung and Miller [51] revisit the calculations of Berger and Coester [48, 49] and examine the effect of the quantization of the pions on the light cone versus at "equal time". With "equal time" quantization, they calculate a roughly flat 8% increase in the Drell-Yan iron cross section over the deuterium cross section. Brown *et al.* [52] argue that with the partial restoration of chiral symmetry, the masses of hadrons made up of light quarks decreases with density. This rescaling leads to altered couplings, which lead to an overall *decrease* in the Drell-Yan cross section in
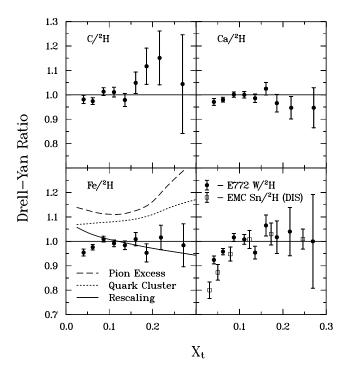
FIG. 7: E772 measurements of the ratio of Drell-Yan cross sections on nuclear targets to deuterium as a function of x_{target}[39]. Except for shadowing at small x, there are no apparent nuclear effects within the limits of the statistical uncertainty.
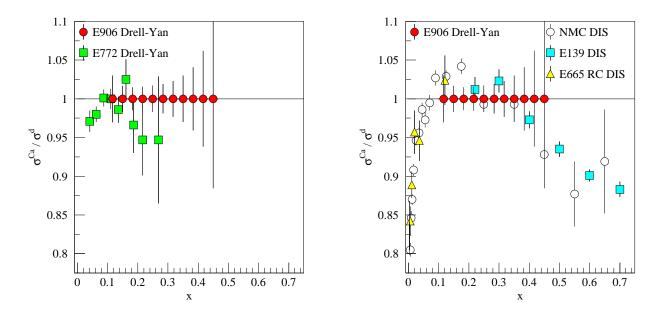
FIG. 8: FNAL E772 Drell-Yan results (left) and a compilation of deep inelastic scattering (right) results on the ratio of cross sections of calcium to deuterium, compared with the statistical uncertainties of the proposed measurement arbitrarily plotted at 1.0). The systematic error is expected to be less than 1%.
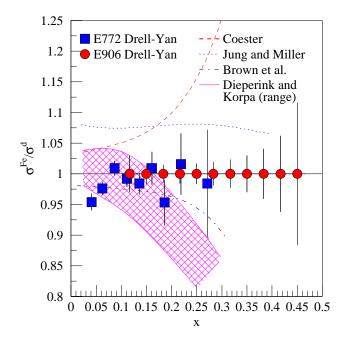
FIG. 9: Ratio of iron to deuterium Drell-Yan cross sections as measured by Fermilab E772 (green squares)[39]. The expected sensitivity of the E906 experiment is shown as red circles, arbitrarily plotted at 1. To illustrate the level of effects expected, curves based on several different representative models are also plotted. The difference between the models is discussed in the text. The red dashed curve represents predictions by Berger and Coester [48–50] including both nuclear motion and pion contributions of $\bar{u}$ in iron to $\bar{u}$ in deuterium. After the E772 data became available, revised calculations by Jung and Miller [51] (green solid curve) and Dieperink and Korpa [53] (the range indicated by the black dotted curves) and Brown *et al.* [52] (blue dot-dashed curve) were made. The E906 data will clearly be able to see the effects predicted by these calculations.

nuclei. Dieperink and Korpa [53] also argue that the Drell-Yan cross section ratio should decrease in a nucleus. Their arguments are based on particle- and delta-hole model, which results in a strong distortion of the free pion structure function. Finally, Smith and Brown [54] are able to simultaneously describe the EMC effect and the E772 data using a chiral quark-soliton model, which predicts essentially no nuclear effect in Drell-Yan. Unfortunately, for $x > 0.2$, the E772 statistical uncertainties allow some freedom for these models and is not able to distinguish between them. At $x \approx 0.3$ these newer models have nuclear effects of the order 5 to 15% in the Drell-Yan ratio. E906 will provide the sensitivity needed to see the reduction in the nuclear sea distributions predicted in the Q^2 rescaling models [52] and differentiate this from other models which predict an enhancement in the Drell-Yan ratio, as illustrated in Fig. 9.

Finally, the nuclear target data will constrain possible nuclear effects in the $\bar{d}_p/\bar{u}_p$ measurement.

A large rise in the nuclear ratio would provide an important signal that nuclear effects may be important in the deuterium to hydrogen ratio.

2.4.   Partonic Energy Loss

Parton energy loss is a fundamental process within QCD that has significant impact on the physics of relativistic heavy-ion collisions. The magnitude of the initial energy loss in the heavy-ion collision determines the ultimate density that is achieved. Furthermore, anomalous energy loss of fast partons ("jet quenching") has been identified as a tool to measure the gluon density of the high temperature medium which is created at RHIC and a possible signature for the creation of a quark-gluon plasma.

The PHENIX collaboration [55] has reported evidence for the suppression of high-p_T π^0s and both the STAR [56] and PHENIX [57] collaborations have reported evidence for the suppression of high-p_T charged hadrons in Au-Au collisions at $\sqrt{s_{NN}} = 130$ GeV. The STAR collaboration [58] has also identified large azimuthal anisotropies in the production of high-p_T charged hadrons in Au-Au collisions at $\sqrt{s_{NN}} = 130$ GeV. The PHENIX data now reach to $p_T \approx 10$ GeV and include a π^0 reference spectrum taken with the same detector. The STAR data now reach to $p_T \approx 12$ GeV and include evidence for the suppression of back-to-back jets in central Au-Au collisions [59]. These results, taken together, provide clear evidence for energy loss of high-p_T partons or their hadronic fragments in the high-density medium produced in Au-Au collisions at RHIC. However, detailed interpretation will require understanding several additional competing effects—including initial- and final-state multiple scattering, gluon shadowing, radial and elliptical flow—as well as the energy loss of fast partons in normal nuclear matter.

The Drell-Yan process provides an excellent means to study the interactions of fast partons traversing cold nuclei since the dimuon in the final state does not interact strongly with the partons in the medium. Thus, it can be used to estimate the energy loss of fast quarks in cold nuclear matter, thereby establishing a baseline for the energy loss that would be expected during a heavy-ion collision even without formation of a quark-gluon plasma. Both E772 [39] and E866 [16] measured the nuclear dependence of Drell-Yan dimuon production in 800 GeV p-A collisions, and the E866 results have been analyzed to search for evidence of energy loss of the incident quark as it traversed the nucleus prior to the hard scattering [16].

Three different forms for this energy loss have been proposed, each of which can be expressed in

terms of the average change in the incident-parton momentum fraction prior to the collision, Δx_1, as a function of target atomic mass (A). Gavin and Milana [60] adopted a form

$$\Delta x_1 = -\kappa_1 \, x_1 \, A^{1/3}, \tag{12}$$

based on an analogy to the transverse spin asymmetry in direct photon production. Brodsky and Hoyer [61] used an analogy to the photon bremsstrahlung process to obtain a form for gluon radiation, leading to an initial-parton energy loss

$$\Delta x_1 \approx -\frac{\kappa_2}{s} A^{1/3}. \tag{13}$$

They also noted that elastic scattering should make a similar contribution to the energy loss. The formulation developed by Brodsky and Hoyer was extended by Baier *et al.* [62, 63]. They found that the energy loss of sufficiently energetic partons depends on a characteristic length and the broadening of the squared transverse momentum of the parton. For finite nuclei, both factors vary as $A^{1/3}$, so Baier *et al.* predict

$$\Delta x_1 \approx -\frac{\kappa_3}{s} A^{2/3}. \tag{14}$$

In each of these three equations (Eqs. 12, 13 and 14) κ is a constant that sets the overall scale of the energy loss.

In all three cases, the signature for incident-parton energy loss is a modification of the Drell-Yan cross section per nucleon on a heavy nucleus as a function of x_1. However, the E866 nuclear dependence data were taken at relatively small x_2 ($\langle x_2 \rangle = 0.038$), where DIS experiments show clear evidence for nuclear shadowing. In addition, the Drell-Yan acceptance in E866 introduced a strong anti-correlation between x_1 and x_2. Thus, it was essential to correct the data for the effects of nuclear shadowing. The EKS98 shadowing parameterization [64, 65] was designed to fit the observed nuclear dependence of deep-inelastic scattering over a broad range of x and the nuclear dependence of Drell-Yan scattering observed by E772 at $x_2 > 0.08$, while simultaneously conserving baryon number and momentum. It gives a very good description of the nuclear dependence of the Drell-Yan cross section per nucleon at small x_2 observed in E866. Thus, EKS98 was used to correct the E866 data for nuclear shadowing.

The small residual nuclear dependence observed in E866 as a function of x_1 was then used to set upper limits on the incident-parton energy loss in each of the three models above. The fits are shown in Fig. 10. E866 found that the fractional energy loss of the incident quarks is less than
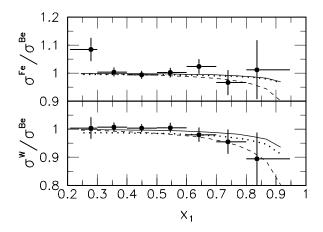
FIG. 10: E866 ratios of the Drell-Yan cross section per nucleon versus x_1 for Fe/Be (upper panel) and W/Be (lower panel), corrected for shadowing [16]. The solid curves are the best fit using the energy loss form in Eq. 12, and the dashed curves show the one standard deviation upper limits. The dotted curves show the one standard deviation upper limits using the energy loss form in Eq. 14. The upper limit curves using the energy loss form in Eq. 13 are essentially identical to those using the form in Eq. 14.

0.14%/fm ($1\,\sigma$), when using the model of Gavin and Milana. The incident quarks lose energy at a constant rate of less than 0.44 GeV/fm, when using the model of Brodsky and Hoyer, and the observed energy loss of the incident quarks within the model of Baier *et al.* is $\Delta E < 0.046$ GeV/fm^2 $\times L^2$, where L is the quark propagation length through the nucleus. These upper limits on the energy loss are tighter than previous direct constraints.

An alternative approach has been adopted to determine incident-parton energy loss in a recent reanalysis [66] of the E772 and E866 Drell-Yan nuclear dependence studies. This work fits the Drell-Yan nuclear dependence with the combination of a "first-principles" calculation of the nuclear shadowing in Drell-Yan scattering, based on the coherence length of $q \leftrightarrow q\gamma^*$ fluctuations as observed in the target nucleus rest frame, and a colored-string model for parton energy loss. It concludes that the average incident-parton energy loss is $2.73 \pm 0.37 \pm 0.5$ GeV/fm, in clear contradiction to the less than 0.44 GeV/fm result from the most similar E866 analysis. Approximately half of this difference originates from different treatments of the path length through the nuclear matter [67]. The E866 analysis took the path length to be the average propagation distance within the nucleus prior to the hard scatter that produces the Drell-Yan pair, whereas the recent E772 and E866 data reanalysis takes the path length to be the average propagation distance from the first inelastic scattering, when the colored string is formed, until the hard scatter occurs. The rest of the difference can be traced ultimately to the two different treatments of nuclear shadow-

ing. In particular, the "first-principles" calculation predicts much less shadowing than the EKS98 parametrization and, thus, requires considerably more energy loss to fit the experimental data.

At present, it is unclear which approach to evaluate the shadowing is more appropriate for the existing experiments. The coherence-length approach is based on well-defined QCD principles and is particularly attractive at very small x_2. Similar calculations of shadowing in deep-inelastic scattering do a very good job of describing the data at small x. However, for $x > 0.04$, the coherence-length calculations fail to reproduce the nuclear dependence observed in deep-inelastic scattering. This is notable because most of the E772 Drell-Yan events and nearly half of the E866 Drell-Yan events have $x_2 > 0.04$. Furthermore, the large apparent energy loss found using the coherence-length approach appears to be inconsistent with the initial results from RHIC. It is also inconsistent with two other recent determinations of the energy loss of fast quarks in cold nuclear matter: 0.20 ± 0.15 GeV/fm from a combined fit to the E866 (p-A) and NA3 (π^--A) Drell-Yan data [68] and 0.5 GeV/fm from a study of semi-inclusive DIS data from HERMES [69].

In contrast to the "first-principles" shadowing calculations, EKS98 is based primarily on *ad hoc* parameterizations of the nuclear dependence seen in deep-inelastic scattering that have only limited theoretical motivation, but which nonetheless describe its observed x and Q^2 dependence quite well. But, as noted above, EKS98 also included E772 Drell-Yan data at $x_2 > 0.08$ in its fit. While most of the E866 statistics had x_2 well below this, there is a concern that some incident-quark energy loss may have been folded into the EKS98 shadowing fit inadvertently, thus obscuring the effect of energy loss during the E866 analysis. However, if the E866 data had been analyzed with a new shadowing parametrization that is based solely on DIS input data [70], rather than EKS98, the conclusions would have been similar to those in [16].

The best way to resolve this question is to perform a second Drell-Yan nuclear dependence study at a substantially lower beam energy. This amplifies the expected effect substantially, as seen in the $1/s$ dependence of Eqs. 13 and 14. Main Injector energies are ideal for such a study. One would like to observe the nuclear dependence of Drell-Yan scattering as a function of x_1 for moderate values of x_2, where all models predict the cross section per nucleon should vary from nucleus to nucleus by no more than a few percent. The experiment will measure the x_1 dependence for those events that have $0.1 < x_2 < 0.2$. This x_2 region is comfortably above the traditional shadowing domain and below the momenta where the EMC effect and/or Fermi motion may modify the target antiquark densities. It was also investigated with moderate statistics by E772, providing a basis for comparison of events at comparable x_2 but quite different x_1. Figure 11 shows the statistical
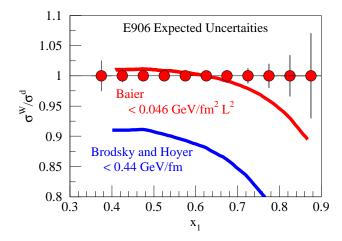
FIG. 11: Expected statistical accuracy of E906 for the ratio of the Drell-Yan cross sections per nucleon for W/D vs. x_1. Only events with $0.1 < x_2 < 0.2$ and effective mass above 4.2 GeV have been considered. The systematic uncertainty in the cross section ratios is expected to be approximately 1%. The cross section ratios have arbitrarily been plotted at 1. The solid curve shows the expected cross section ratio for a fractional energy loss of 0.14%/fm (Eq. 12). The dashed curve shows the expected cross section ratio for a constant energy loss of 0.44 GeV/fm (Eq. 13), based on the procedures used to estimate path lengths in the E866 analysis [16].

accuracy that will be obtained for the Drell-Yan nuclear dependence as a function of x_1 during E906. The systematic uncertainty in the cross section ratios are expected to be approximately 1%. The cross section ratios in the figure have arbitrarily been set equal to 1. Only events which will satisfy the trigger and pass the target and dump cuts that have $0.1 < x_2 < 0.2$ and effective mass above 4.2 GeV have been included. Comparable statistics will be obtained for the cross section ratios for the other two nuclear targets. To demonstrate the sensitivity of this measurement to incident-parton energy loss, the x_1 dependence that one would expect for an energy loss equal to the upper limits found by E866 for models (12) and (13) above and for an energy loss equal to the result found from the "first-principles" reanalysis of E772 and E866 data has been calculated. The expected x_1 dependence of the cross section ratio per nucleon for W/D in model (14) is similar to that for model (13), but the two models will be distinguished by their different predicted A dependences. Overall, E906 will be a factor of 5 to 10 more sensitive to incident-parton energy loss than E772 or E866. The ultimate sensitivity will be limited by our ability to separate incident-parton energy loss effects from nuclear modifications of the target antiquark distributions, which will be determined largely by the results of the target antiquark studies that are also planned for E906.

3. EXPERIMENTAL APPARATUS

The design of the experimental apparatus leans heavily on the collective experience of Fermilab E605, E772, E789 and E866/NuSea for the best technique to handle high luminosities in fixed target Drell-Yan experiments. The apparatus is optimized for events with large x_2 and $x_F \approx 0.2$. For scale, the muons generated by a 7 GeV virtual photon with $x_F = 0.2$ which decay perpendicular to the direction of motion (in the virtual photon rest frame) will in the laboratory have momenta of 33 GeV, an opening angle of 210 mr and transverse momenta of 3.5 GeV. A sketch of the apparatus showing trajectories for muons is shown in Figs. 12 (bend plane view) and 13. The key features of the apparatus are:

- Relatively short (<15% interaction length, L_I) targets to minimize secondary reactions in the target.

- Two independent magnetic field volumes, one to focus the high transverse momentum muons and defocus low transverse momentum muons and one to measure the muon momenta.

- A 15 L_I hadron absorber to remove high transverse momentum hadrons.

- A 30 L_I beam dump at the entrance of the first magnet.

- Zinc and concrete walls for muon identification at the rear of the apparatus (located after Station 3 and between the planes of Station 4).

- Maximum use of existing equipment consistent with the physics goals.

While the lower beam energy is a great advantage in terms of cross section and background rates and statistics, it has two disadvantages relative to 800 GeV experiments.

- The corresponding lower particle energies lead to increased probabilities for muonic decay of the produced hadrons. This is partially compensated by reducing the target-to-hadron-absorber distance to 1.3–1.8 m.

- The lower energy muons multiple scatter more easily in the hadron absorber.

As will be discussed below, much of the apparatus consists of equipment recycled from previous experiments. Only the first magnet requires a significant construction effort.
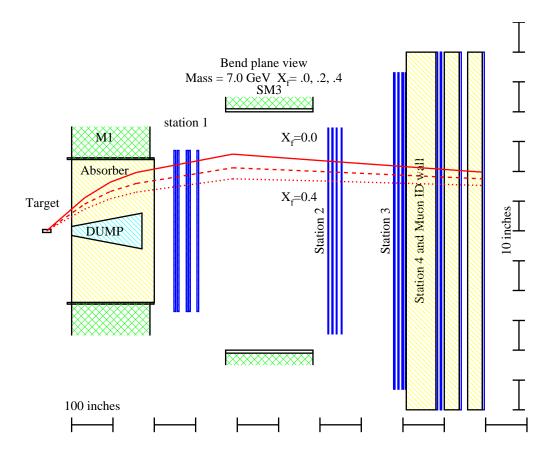
FIG. 12: Bend plane view of the trajectories of one of the two muons resulting from the muonic decay of a 7 GeV virtual photon (which has x_F of 0.0, 0.2 or 0.4) in an 8 T-m spectrometer.

3.1. Beam and Targets

The requirements for the beam are 2×10^{12} protons/s and a total of 5.2×10^{18} protons on target[3]. The exact spill cycle remains to be worked out, but one possible way to achieve this in a two year run is by delivering 10^{13} protons in a 5 s slow extraction spill every minute [71]. The maximum beam spot size of 5 mm vertical by 10 mm horizontal and maximum divergence of 2 mr in each direction. The primary beam will stop in a 170" long trapezoidal copper beam dump starting with a 3" vertical height at z=0 extending to a 12" vertical height at z=170". Since the dump will absorb an average of 6400 watts of beam power, it will be water cooled with a closed loop recirculation system similar to the E866/NuSea beam dump.

---

[3] The integrated number of protons on target is the same as in the original proposal. To minimize the impact on other proton users at Fermilab, the instantaneous proton intensity has been doubled, thus requiring half the number of accelerator cycles to deliver the needed integrated luminosity.
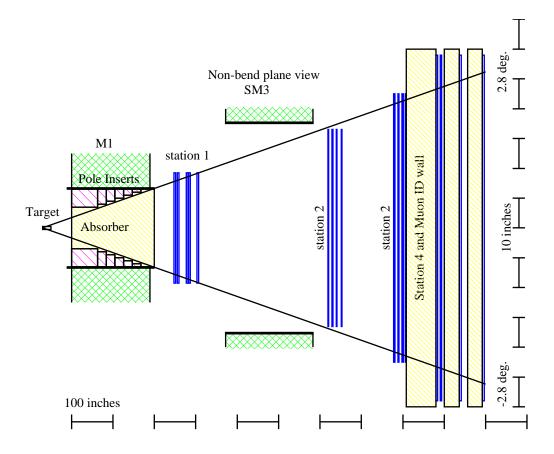
FIG. 13: Non-bend plane view in an 8 T-m spectrometer. Only muons which pass around the beam dump in the bend plane contribute to the acceptance and so the beam dump is not shown.

The experiment will use 50.8 cm long liquid hydrogen and deuterium targets, three nuclear targets of approximately 10 gm/cm^2 thickness and a dummy liquid target cell. The targets would be remotely interchanged. In E866/NuSea, this was done every 5 spills in the 40 s between spills. A similar rotation is envisioned for E906/Drell-Yan, depending on the final accelerator cycle. The target rotation would be such that the hydrogen target will be in the beam 35% of the time; deuterium–26%, dummy liquid cell–4% and nuclear targets–35% (split between the three nuclear targets). The exact choice of nuclear targets has not been made but they are likely to be carbon, calcium or iron and tungsten. An advantage of iron would be a more direct comparison with the CCFR data. Tungsten would extend the nuclear dependence studies to a heavy nucleus, especially for the energy loss studies. Fermilab has been asked to provide the beam line instrumentation and suitable targets (either reusing the E866/NuSea targets or a new target system).

3.2. Magnets

The first magnet of the spectrometer focuses the high transverse momentum muons into the apparatus' acceptance and bends low momentum muons out of the acceptance. The optimal performance is obtained with a large-aperture, vertical-bend magnet [48" (y) by 26" (x)] whose transverse momentum, p_T, kick is approximately 2.5 GeV ($\approx$ 8.4 T-m). While reasonable Drell-Yan acceptance may be retained for lower field integrals, provided the aperture of the downstream spectrometer is large enough, the singles rates dramatically increase to an unacceptable level. Even with the present design the experiment must be prepared for 100 MHz instantaneous rates in the first set of wire chambers.

The change in beam energy (boost) from 800 GeV in E866/NuSea to 120 GeV in E906/Drell-Yan means that the 570-inch "SM12" magnet used by E866/NuSea is not appropriate for this experiment. Instead, a new magnet must be constructed. A 189" long 8 T-m large aperture magnet can be constructed using 1/3 of the iron from SM12 and new coils, following the same general principles as the SM3 magnet. The characteristics of this magnet are given in Tab. I. Iron inserts will provide a tapered horizontal aperture of 98 mr opening angle tailored to the aperture of the second magnet. With such a magnet, there appear to be no experimental barriers to completing the measurement proposed here.

The second magnet must provide the accurate momentum determination with a large acceptance. The SM3 magnet will be used for this purpose. (This magnet was used in the original Drell-Yan spectrometer.) Some of the characteristics of SM3 are also given in Tab. I. For radiation protection purposes, the spectrometer, like the previous Meson-East spectrometer, will need to be vertically bending. SM3 is already in this orientation.

The aperture around the beam dump in the first magnet will be filled with a graded hadron absorber. GEANT-based Monte Carlo's are being used to optimize the configuration of the absorber. One possible configuration would be 80" of graphite, followed by 40" of copper then 40" of graphite and 40" of Borated Polyethylene. Al_2O_3 may be used in place of some of the Cu. The 40" of copper helps to eliminate particles which escape from the dump. The instantaneous single rates at each of the detector stations are given in Tab. II The dominant single contribution is muons produced by the decays of hadrons in the dump.

The muons will lose approximately 3.5 GeV in energy passing through the absorber and multiple scatter by an average angle of $170/p_\mu$ mr (p_μ is the muon's momentum in GeV). This level of multiple

TABLE I: The characteristics of the proposed M1 and the SM3 magnet. The M1 horizontal aperture is without the pole inserts.

Property	M1	SM3
Length	189 in	211 in
Width	95 in	147 in
Height	198 in	198 in
Vertical Aperture	48 in (123 cm)	63 in (160 cm)
Horizontal Aperture	26 in (66 cm)	70 in (178 cm)
Field Integral	8.14 T-m	3.0 T-m
Ampere-Turns	670,000	800,000
Current	2,400 Amp	4,200 Amp
Power	580 kWatt	400 kWatt
Inlet Water Temperature	38°C	38°C
Temperature Rise	25°C	25°C
Water Flow	90 gal/min	60 gal/min
Weight:		
Pole Inserts	9.5 t	10 t
Coils	19 t	40 t
Return Yoke	420 t	300 t
Total	450 t	350 t

TABLE II: Wire Chamber Specifications and Singles Rates

Station	Type	x size (cm)	y size (cm)	wire spacing (mm)	wire orientations	Number of Channels	Expected Singles Rates (MHz)
1	MWPC	94	137.2	2.0	Y,Y',U,U',V,V'	5500	80
2	DC	137.7	149.9	10.2	Y,Y',U,U',V,V'	1000	20
3	DC	203.0	162.4	20.3	Y,Y',U,U',V,V'	700	4
4	Prop. Tubes	250.0	250.0	50.8	Y, Y', X, X'	400	8

scattering will still permit acceptable virtual photon mass resolution (approximately 240 MeV) and acceptable vertex resolution to separate target and beam dump events for muon energies greater than 15 GeV. Due to the long target length relative to the target-to-absorber distance, the target position provides minimal additional track constraints for the mass measurement.

3.3. Tracking Chambers

The possibly high instantaneous rates at Station 1 require it to be able to handle rates up to 100 MHz. The E866/NuSea Station 1 drift chambers would not be able to handle these rates. Instead, Multi-Wire-Proportional-Chambers (MWPCs) with a 2 mm wire spacing will be built. Station 1 would consist of 6 planes, 2 measuring Y, and 2 each measuring U and V with stereo angles of $\pm 14.0°$. Existing E871 preamplifier-discriminator-readout would be used. Each of these wire chambers has 3 rf bucket hit resolution and would run with a fast gas (CF_4/isobutane, 80:20). The readout would consist of 5500 channels of coincidence registers. All the electronics and readout currently exist (E871 has 20000 wire chamber channels). As an alternative, the possibility of using a combination of E605 and E871 MWPCs exists, but the geometrical coverage is not optimal, with a dead zone along $x = 0$.

Stations 2 and 3 would use the existing E605/E772/E866 drift chamber Stations 2 and 3. They are capable of 250 μm resolution with Ar/Ethane (50:50) gas. The stereo angle is $\pm$ 14 degrees. Existing preamplifiers and discriminators would be adequate. Some of the electronic crates in which these components are mounted were replaced prior to E866/NuSea's run in 1996. The remainder of the crates will be replaced. A 1700 channel multi-hit TDC system is required for good efficiency and rate capabilities. A more than sufficient number of LRS 3377 modules in the Fermilab PERP electronics pool and should be available [72].

Station 4 would be constructed of new, commercially available, limited streamer tubes with a 2 inch pitch operated in proportional mode, similar to those used by the PHENIX detector's end-cap muon id system. Existing amplifiers and discriminators from E866/NuSea will be used. The readout would be identical to the MWPC's and add 400 channels to the electronics and coincidence register total.

The rate dependence of the pattern recognition efficiency has been studied with Monte Carlo simulations to ensure that this choice of chamber configuration is acceptable. With the rates given

in Tab. II, there is only a 4% decrease in efficiency, on the same scale as the level of rate dependent effects which were handled in E866/NuSea.

3.4. Scintillator Hodoscopes

Scintillator hodoscope planes will provide the hit information for the hardware trigger system, just as they did in E866/NuSea. Each of the four tracking station will have a y-measuring hodoscope plane associated with it. Each plane will have a total of 32 channels, separated into two groups of 16 channels for the left ($x > 0$) and right ($x < 0$) sides of the detector. There will be x hodoscope planes associated with detector Stations 1 and 2, plus two additional planes as part of Station 4. They will contain 32 channels apiece, separated into 16 channels for the lower half of the spectrometer ($y < 0$) and 16 channels for the upper half ($y > 0$). This segmentation will provide a logical division of each hodoscope plane into quadrants, allowing the trigger system to place tighter geometric constraints on the tracks than was done during E866/NuSea.

All of the scintillators within a given y hodoscope plane will be the same size. The individual scintillators within hodoscope planes X4A and X4B will all be the same angular size. In contrast, the four X1 and four X2 scintillators closest to $x = 0$ will subtend half the angular range, and the scintillators furthest from $x = 0$ will subtend 1.5 times the angular range of the X4A and X4B scintillators and the remaining X1 and X2 scintillators. This segmentation minimizes the number of hodoscope channels in Stations 1 and 2 that may be in coincidence with given channels in X4A and X4B, after accounting for the multiple scattering of the muons through the various absorbers in the spectrometer.

While many of the hodoscopes could be fabricated primarily by re-cutting and polishing the existing E866/NuSea scintillators to the sizes required for the new spectrometer, it is safer, given their age[4], to plan on constructing new scintillators and light guides for this experiment. The phototubes and bases from the existing E866/NuSea spectrometer will be reused (approximately 160 units). An additional 220 phototubes and bases are needed. These will be recovered from Argonne/HEP's contribution to the Zeus detector at DESY when it is decommissioned in the fall

---

[4] The scintillator in Stations 3 and 4 were installed as part of E605 in 1982. The scintillator in Station 2 is from 1989, and examination scintillator left over from that installation show signs of crazing. Station 1 is of insufficient size to be reused.

of 2007. The existing E866/NuSea high voltage distribution systems will suffice to power the eight hodoscope planes.

For E866/NuSea, the anode signals from each phototube were sent to LeCroy 4416 leading-edge discriminators. The discriminator outputs were reshaped by custom synchronizer/stretcher modules to provide clean, single RF bucket time resolution for all hodoscope planes except Station 4, which had slightly worse than single bucket resolution. The higher background rates anticipated at the Main Injector due to the increased beam current make it very important to achieve clean, single RF bucket time resolution for all hodoscope planes. Given past experience, this should be straightforward with the existing discriminators for the hodoscopes in Stations 1 and 2, and for the X4A and X4B planes. The longest scintillators in the spectrometer, those for Y4, will be only 7" shorter than the Station 4 scintillators during E866/NuSea and phototubes will be placed on each end of these scintillators. With the double-ended readout and mean timers single bucket resolution will be achieved. Enough synchronizer/stretcher modules are available to instrument the entire new spectrometer.

3.5. Muon Identification

Final muon identification is provided with an absorber wall, 81 cm of concrete followed by 92 cm of zinc and 10 cm of lead, followed by 2 planes of streamer tubes and the X4A scintillators, then 92 cm of concrete followed by the Y4 and X4B scintillators and finally 92 cm of concrete followed by 2 planes of streamer tubes. The present E866/NuSea muon identification walls provide enough material for the smaller E906/Drell-Yan wall [41].

3.6. Trigger

The hardware trigger system will examine the scintillator hodoscope hits to identify patterns characteristic of high mass muon pairs produced in the target. It will be conceptually similar to the system that was developed for E866/NuSea [73]. However, it will be enhanced substantially compared with the previous system, primarily to improve its ability to reject random coincidences that appear to form a candidate high p_T muon track. Such random coincidences represented over half of the apparent muon tracks observed during the E866/NuSea intermediate mass $\bar{d}/\bar{u}$ running, and the background rates in the spectrometer due to soft muons are expected to be even higher at the Main Injector. The trigger modifications will also permit the implementation of two-dimensional

masking of wire chamber hits during event analysis, based on the active hodoscope roads, which will reduce the combinatorics in the wire chamber track finding. Notably, this will minimize the frequency of "hit-bank" and "track-bank" overflows, one of the sources of rate-dependent reconstruction inefficiency that we encountered during E866/NuSea. Finally, the trigger modifications will allow for the replacement of a number of custom CAMAC modules from the E866/NuSea trigger system that are now nearly 20 years old with new, more reliable and flexible units.

Electronically, the hardware trigger will consist of a single decision stage, implemented as a three-step parallel pipeline. In the first step, the outputs from the hodoscope synchronizer/stretcher modules will be routed to a set of logic modules based on commercially available FPGAs (Field Programmable Gate Arrays)[5]. The logic will identify four-fold Y1-Y2-Y3-Y4 coincidences characteristic of high p_T single muons produced in the target. Each time they observe a candidate track, they will output a bit indicating its charge, the side of the spectrometer (left or right) where it is located, the quadrant the track passed through at Y1, and the actual y location of the track at Y4. In general, Y1-Y2-Y4 triple coincidences would suffice since the spectrometer analyzing magnet is located between Stations 1 and 2, and that is in fact how candidate tracks were identified during E866/NuSea. Adding the extra constraint that the appropriate channel of Y3 must have a hit will help reject apparent tracks that actually consist of a random coincidence between hits in Stations 1 and 2 due to one muon and a hit in Station 4 due to another.

An additional FPGA logic unit will be dedicated to identifying candidate tracks originating from the target that include coincidences among at least three of the four planes X1-X2-X4A-X4B. Each time they observe a candidate track, they will output a bit indicating the side of the spectrometer where it is located, the quadrant the track passed through at X1 and X2, and the actual x location of the track at X4A and X4B. This represents a significant upgrading of the tracking capability of the hardware trigger in the x direction, compared with E866/NuSea, and will permit full two-dimensional constraints on the tracks. It will also make continuous monitoring of the efficiency of the y hodoscopes practical. This will be important because the ability to average over long-term variations in the spectrometer efficiency between targets will be reduced at the Main Injector, since it will be difficult to change amongst the various targets as frequently as was done during E866/NuSea. In contrast, for E866/NuSea special hodoscope efficiency studies were run every

---

[5] In the original proposal, this was going to be implemented in LeCroy 2367 modules, which are now no longer available. Fortunately, in the meantime, the cost of FPGAs has dramatically decreased and their speed has increased.

few weeks. They consisted of a series of runs utilizing a special trigger configuration, sequentially turning off the high voltage on sets of x hodoscopes near the center of the spectrometer.

The second step in the trigger pipeline will combine the x and y tracking results from the first step to identify events with candidate high p_T muons present. This will be done in a pair logic modules modules, one dedicated to tracks on the left side of the spectrometer and one dedicated to tracks on the right side. The candidate muons will be characterized according to their charge, the side of the spectrometer on which they are located, and a rough measure of their p_T. Events will also be tagged that appear to have two muons with opposite charges present on the same side of the spectrometer.

In parallel with the first two steps of the main trigger sequence, OR's of all the scintillators on each side of each plane will be generated and routed to a Track Correlator [73] to generate simple cosmic ray and noise triggers for diagnostic purposes. This procedure was utilized during E866/NuSea, and the same CAMAC and NIM electronics will be reused at the Main Injector.

The final step in the trigger pipeline will generate the actual triggers, handle the experiment busy logic, and strobe the read-out electronics. This step will either be performed with one logic module or with the Track Correlators and Master Trigger OR that were designed and constructed for the E866/NuSea hardware trigger [73]. The primary physics trigger will consist of a coincidence between two candidate $x - y$ tracks of opposite charges, on either the same or opposite sides of the spectrometer. If the background trigger rate due to low mass muon pairs is higher than desirable, a rough measurement of the p_T for the two muons from the previous step may be added to provide a crude effective mass cut on the muon pair in hardware. A similar procedure, but with less granularity than anticipated with the new trigger system, was adopted for several of the data sets taken during E866/NuSea. It reduced the raw trigger rate during the E866/NuSea intermediate mass $\bar{d}/\bar{u}$ data taking by a factor of three, with essentially no reduction in efficiency for the Drell-Yan muon pairs of interest. Two triggers will be used to determine the rate of random coincidences between two muon tracks in the same RF bucket, both of which originate from the target and, thus, are indistinguishable from a real Drell-Yan muon pair. One of these triggers will record events that contain two muons of the same charge when they are located on opposite sides of the spectrometer, while the other will record a prescaled set of single-muon events. E866/NuSea has demonstrated that an excellent simulation of the random coincidence background can be obtained by combining muons from single-muon triggers into pairs, then normalizing their number to the observed rate of like-sign coincidences. Two additional triggers will select prescaled samples of events that contain
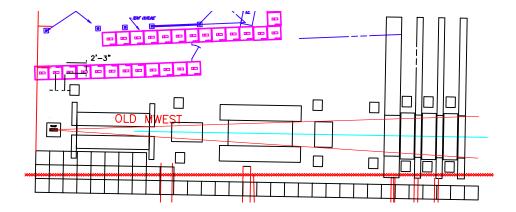
FIG. 14: This figure shows the layout of the MWest part of the Meson area with the E906 spectrometer in place.

a candidate track in either the x or y direction, but not necessarily both. The events with x tracks will be used to monitor the absolute efficiencies of the y hodoscopes, and the events with y tracks will be used to monitor the absolute efficiencies of the x hodoscopes. The last trigger will provide a luminosity-weighted read-out of all detector elements during random RF buckets, independent of the status of any of the spectrometer hodoscopes. This will be used to provide an unbiased measure of the background occupancy rates throughout the spectrometer, which are very important for estimating rate-dependent reconstruction inefficiencies.

3.7. Spectrometer Location

The experiment as proposed in 1999 and 2001 was to take place in the Meson East (MEast) experimental area where E772, E789 and E866 had run. This had the advantage that much of the infrastructure, including the beam line, suitable foundations for both dipole magnets, etc. was already in place. In 2005, however, an effort was begun to transform MEast into a Superconducting Cryo-Module Test Facility. E906 was tentatively moved to the MWest beam-line. While not the ideal location for E906 (it is rather cramped as compared with the previous location in MEast) there is sufficient room for the spectrometer and it will work as shown in Fig. 14. There is clearly some additional cost to Fermilab because of this move, which was presumably balanced against the need for to place the Superconducting Cryo-Module Text Facility in MEast. The recommissioning of this beam line and the location of the experiment is the subject of a recently completed Meson Beam Task Force study chaired by Dave Christian [71].

3.8. Monte Carlo of Trigger and Spectrometer Rates

Thorough Monte Carlo simulations have been done to determine both the detector response and resolution, and spectrometer and trigger rates. Two different Monte Carlo codes have been used for these simulations. The primary one is a modified version of the "Fast Monte Carlo" that was originally written to estimate acceptances in E605/E772/E789/E866. It has now been modified to simulate the detector configuration for this experiment–E906/Drell-Yan. This Monte Carlo simulates muons from Drell-Yan, resonance production (J/ψ, ψ', Υ, $\Upsilon(2S)$, $\Upsilon(3S)$), and π, K and charmed meson decays. It can track single muons or pairs through the entire spectrometer in order to estimate signal and background rates with realistic hardware trigger simulation. It also simulates the traceback of the muon tracks to the target so that realistic tracking cuts may be imposed and the ultimate resolutions of the spectrometer can be estimated. The details of the thrown spectra and assumed cross sections can be found elsewhere [74]. The second code is a GEANT-based Monte Carlo. This code was written to optimize the design of the hadron absorber wall. Unlike the first code, this Monte Carlo only tracks particles as far as Station 1. However, it tracks all particles which arise from proton interactions in the targets and beam dumps, rather than just muons, so it is quite useful for configuring the hadron absorber that will fill the aperture of the large M1 magnet. Both codes have been demonstrated to give a reasonable description of the rates that were observed during E866/NuSea, and they give consistent results for the flux of muons with momenta above 3 GeV that should be present in Station 1 at the Main Injector.

The Fast Monte Carlo code has been verified through a number of further tests. The simplified muon traceback to the target has been checked by verifying that it reproduces observed resolutions during E866/NuSea. For example, the predicted and observed J/ψ mass resolutions during the E866/NuSea large-x_F nuclear dependence study agree to within 10%.

The Monte Carlo has been used to estimate the trigger rates. The rates of muon pairs from Drell-Yan and resonance production originating in either the target or the dump have been simulated for the equivalent of 10^3 to 10^5 spill-second at an assumed intensity of 2×10^{12} protons per spill-second. The rate due to Drell-Yan pairs off the LH_2 target is 5/spill/s, with approximately one third of these passing the tracking and effective mass cuts. The total real rate is expected to be approximately 200 events per 2×10^{12} protons, with approximately 15% of these passing trigger matrix cuts, depending on the target. The vast majority of the events are from J/ψ's produced in the beam dump and do not pass trigger requirements. The yield of muon pairs from $D\bar{D}$ production

is very small. At $\sqrt{s} = 15$ GeV, there will be very few Υ events ($m_\Upsilon = 9.5$ GeV) over the life of the experiment.

In addition to the real pairs, there will be a significant number of triggers from random co-incidences of two independent muon tracks. When running with the liquid hydrogen target, the primary source of background single muons will be π and K decay-in-flight in the beam dump. When running with the liquid deuterium target, the π and K decay-in-flight background from the target will be slightly larger than that from the dump. The total rate of single muons traversing the detector and passing the trigger matrix tracking will be approximately 100 kHz with the LH_2 target and 150 kHz with the LD_2 target (both cases include tracks originating in the beam dump). In each case, the Monte Carlo predicts that the ratio of positive to negative muons will be approximately 2:1, as shown in Tab. III. Using a time resolution equivalent to the Main Injector clock frequency of 53 MHz, this leads to estimates of 50 random dimuon triggers per spill for the LH_2 target and 100 random triggers per spill for the LD_2 target, counting all random opposite-sign pairs and the random like-sign pairs that have one muon on each side of the spectrometer. These random trigger rates do not include the additional suppression that will be obtained by constraining the apparent mass of the pair in hardware. Experience from E866/NuSea indicated that these random pairs will have a mass spectrum strongly peaked at masses near or below the J/ψ.
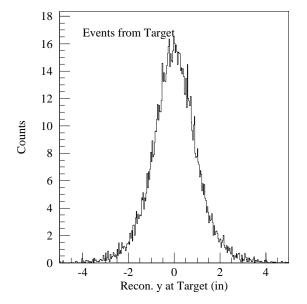
Approximately 80 study triggers per spill will be taken, including prescaled single muons to study the random background, triggers to monitor the efficiency of the hodoscopes, and triggers to investigate any rate-dependence that may be present in the data analysis. Therefore, an overall rate of approximately 200 triggers or less per spill is expected. For planning, a trigger rate of 1 kHz is assumed. With full analysis cuts, the real to random rate is expected to be better than 5 to 1 at all x_2 values, and much better than that at large x_2.

Most of the triggers from the backgrounds are eliminated in the analysis by simple cuts based on whether the track points back to the target and the track's proximity to the beam dump. Histograms of these quantities are shown in Figs. 15 and 16, respectively. To remove tracks originating in the beam dump, an accepted track needed to be at least 5.7 cm off of the beam axis in y at the front face of the dump, and pass within $y = \pm 5.7$ cm at the target. Clearly these restrictions will remove the vast majority of unwanted tracks. In addition, to remove contamination from the ψ and Υ resonance families, the mass of the reconstructed muon pair must be between 4.2 and 8.8 GeV.

In addition to trigger and spectrometer rates, the Monte Carlo was also used to estimate the expected resolution of the detector. For simulated Drell-Yan events which pass the trigger and

TABLE III: Expected single muon rates per 2×10^{12} protons from decay-in-flight mesons which pass through the detector (μ's) and satisfy trigger matrix tracking requirements (Trks.) from liquid hydrogen and deuterium targets and the copper beam dump.

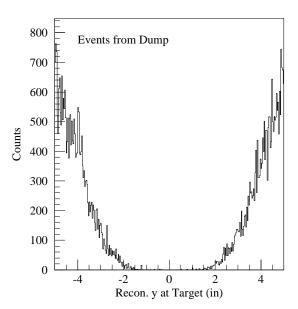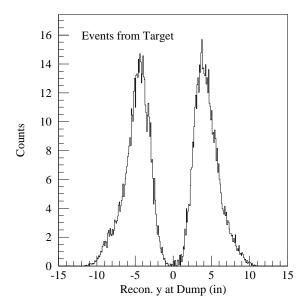|	LH_2 Target		$LD2$ Target		Copper Beam Dump	
	μ's	Trks.	μ's	Trks.	μ's	Trks.
π^+ decay-in-flight	81 k	12 k	195 k	29 k	153 k	13 k
π^- decay-in-flight	35 k	8 k	84 k	20 k	76 k	20 k
K^+ decay-in-flight	63 k	13 k	151 k	31 k	139 k	20 k
K^- decay-in-flight	6 k	3 k	15 k	6 k	18 k	8 k
Total μ^+	144 k	25 k	346 k	60 k	292 k	33 k
Total μ^-	41 k	11 k	99 k	26 k	94 k	28 k

FIG. 15: Distance in y of reconstructed track from target center for Drell-Yan events produced in the target (left) and Drell-Yan events produced in the dump (right). To be considered as an event from the target, *both* tracks must reconstruct within 2.25 inches of $y = 0$.
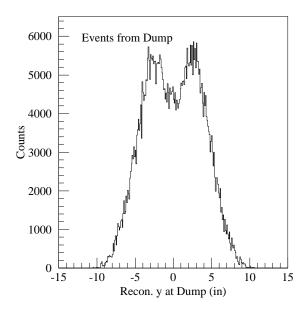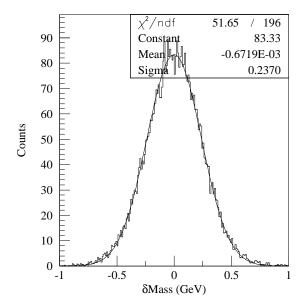
FIG. 16: Distance in y of reconstructed track from the beam dump center at the face of the dump for Drell-Yan produced in the target (left) and Drell-Yan produced in the dump (right). To be considered as an event from the target, *both* tracks must reconstruct at least 2.25 inches away from $y = 0$ at the dump. The double peaked nature of the spectrum of tracks produced in the dump arises from the fact that the dump is an extended source of tracks and the histogram only looked at upstream end of the beam dump.

reconstruction cuts, the expected mass resolution is $\sigma_m = 0.240$ GeV and the x_2 resolution is $\sigma_{x_2} = 0.02$. These are shown in Fig. 17.

3.9. Data Acquisition System

Unlike most of the spectrometer, the data acquisition system will be a departure from the previous linage of Drell-Yan experiments. The readout system for E866/NuSea used the TRANSPORT interface, which was built by the NEVIS electronics group in 1980, to hoist data from custom built TDC's and coincidence registers to tape. Many problems were encountered with that system during the startup of E866/NuSea, and intermittent problems during data acquisition. Both the age of the system and the constraints that it imposes on the data stream require that it be replaced for the new experiment. Because they are to operate in a high rate environment, the drift chambers will be read out with multi-hit TDC's which precludes using the TDC's from the E866/NuSea readout system. As noted in Sec. 3.3 E906/Drell-Yan plans to use LeCroy 3377 multi-hit TDC modules which are available from Fermilab PREP.
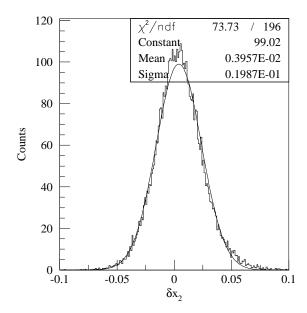
FIG. 17: Expected mass (left) and x_2 (right) resolution for accepted Drell-Yan event using the proposed detector.

Most of readout requirements for the proposed experiment can be met by the front end system that has been assembled for Fermilab experiment E871, which, while it will be over 10 years old when E906/Drell-Yan runs, is available for use by E906/Drell-Yan [75]. The E871 system will provide a high speed readout path for the MWPC's, hodoscopes and proportional tubes configured here. Multi-hit TDC's and the appropriate interface connection to the Processor Bus to read out the drift chambers will be added.

The computer architecture used in E871 is very similar to that planned for this project. Our trigger rates, however, will be much lower than those for E871 and event lengths will be comparable so the dead time using their system should be extremely small. As in E871, data will be moved from front end modules to buffer memory and then written out on tape units. One tape unit should suffice to handle the anticipated bandwidth with average event lengths of less than 1.5 kB and trigger rates less than 1 kHz. Event sampling will be done to monitor wire chamber and hodoscope efficiencies using UNIX based workstations or PC's running Linux.

The DAQ system for this project will follow Fermilab DART standards [76] and use DART software. This represents another break from the E866/NuSea system which did not use DART. The E871 DAQ system uses DART so the front end readout is already compliant with DART standards. With the exception of trigger programming, the remaining system requirements for the new experiment proposed here are already available in DART software packages.

3.10. Analysis

The analysis of the data accumulated in these measurements should be straightforward, both in offline production and for online monitoring. The analysis will be similar to that done for E866/NuSea and would employ a small number of Linux PC's. An estimate of the scope of the analysis task can be made from the expected trigger rate of 1 kHz, estimated event size of 1.5 kB, and a compute time per event of 20 ms/event (on an 180 MHz HP PA8000 used in the E866/NuSea analysis) based on analysis of data in E866/NuSea. Scaling with floating point performance to a 2.5 GHz Pentium IV (a current "commodity" PC) one to two of these CPU's should be able analyze the data in near real-time.

The typical data rate is estimated to be about 0.5 MB/s (easily within the bandwidth of many storage technologies technology) and would result in about 43 GB of data on tape per day, or about 5 TB for the entire run. To analyze these data as fast as they were taken means the networks that support distribution of the data would need to transport in excess of 0.5 MB/s, again easily within the capability of 100 base-T networks.

Since the planned detector system would be conceptually similar to that used in E866/NuSea, the analysis algorithms from E866/NuSea should be applicable to the new experiment. Therefore, much of the old code will be reused. Since much of the raw data format will probably be new the data unpacking parts of the code would probably be rewritten in C or C++, while other parts that need not change may remain in FORTRAN. Since the code already runs on the Fermilab UNIX farms using the Fermilab parallel processing environment (CPS), it should be straightforward to preserve that capability; although, given the speed of current PC's this parallel capacity may not be necessary. CPS is already ported and being used on Linux PC farms at Fermilab.

4. SCHEDULE AND FUNDING

Much of the equipment for the Drell-Yan spectrometer already exists, or is easily and cost effectively obtained. The only exception to this is the fabrication of new coils for the focusing magnet. Funds for the spectrometer upgrade, including the magnet coils, have been requested from DOE/Office of Nuclear Physics (ONP), with additional funding from the NSF. The proposed budget and time line for the spectrometer upgrade will allow E906/Drell-Yan to start production data collection by January 2009. In total, $1,981k was requested from DOE/ONP and $263k from the NSF for the spectrometer upgrade. In anticipation of funding these upgrades, DOE/ONP has

requested that Argonne hold a review of the cost and schedule of this upgrade. This review will take place this December. We have been advised that with Office of Science Budgets close to the President's proposed budget we can expect Office of Nuclear Physics funding for this upgrade when the budget is passed.

The largest new element of the spectrometer is the muon focusing magnet. It will be constructed following the same design principles as the SM12 and SM3 magnets[6] The magnet is designed to reuse whole pieces of the SM12 iron flux return yoke with minimal additional machine work, and Fermilab has reserved sufficient iron from SM12 for the new magnet. The complete cost of producing the new magnet is given in Tab. IV. These are based on a detailed estimate done at Argonne [77] which have been updated with budgetary estimates from coil vendors [78–80]. A brief description of these items is given below.

Magnet Design: The design will be done by the members of the Physics and Advanced Proton Source (APS) divisions at Argonne. This work is already underway, with the anticipation of a bid request for fabrication of the coils in February or March 2007.

Coil—Tooling, Fabrication and Shipping: To obtain an estimate for the cost of fabricating the coils for the new magnet, preliminary designs were sent to five vendors with requests for budgetary estimates. Four of the vendors responded with estimates. The two middle budgetary estimates were considered in determining the cost of the coils. In light of the upcoming review for DOE, these costs are being revisited in detail over the next month as the coils represent two thirds of the upgrade cost.

Magnet Core and Assembly Parts: This encompasses the cost of reworking the SM12 magnet core shelves and iron to meet the geometry of the new magnet.

Magnet Pole Tips: A budgetary estimate based on the rough configuration and amount of steel was obtained. These will be fabricated from steel plates, a readily available, easily priced commodity.

Fermilab has been requested to handle the assembly of the new magnet.

The trigger electronics, scintillator hodoscopes and photomultiplier tubes, Station 1 MWPCs and Station 4 proportional tubes represent the other major costs to the experiment. These costs include:

---

[6] The SM12 magnet from Fermilab E866 is being replaced by this magnet

TABLE IV: This table outlines the overall funding request from DOE/ONP and from the NSF for the experiment. A detailed review of these costs will be held Argonne at the request of DOE/ONP in December.

Magnet Construction

Item	Cost
Magnet Design	$100,000
Coil–Tooling, Fabrication and Shipping	$1,197,000
Magnet Core and Assembly Parts	$75,000
Magnet Pole Tips	$53,000
Magnet Total	$1,425,000

Detector Construction

Item	Cost
Trigger Electronics (NSF)	$134,000
Hodoscopes	$101,000[a]
Tracking Stations	$208,000[b]
Tracking Stations (NSF)	$139,000
Data Acquisition	$48,000
Detector Total DOE/ONP	$357,000
Detector Total NSF	$263,000

[a]Includes savings of $194,000 from recovery of Zeus phototubes.
[b]Does not include possible $24,000 in savings from recovery of HERMES RICH gas circulation system.

Trigger Electronics: The trigger electronics are based on a hodoscope track finding algorithm. This will be accomplished through the use of field programmable gate arrays (FPGAs). These are now readily available and are already widely used particle and nuclear physics experiments. FPGAs are ideally suited for this task. Rutgers, with input from Texas A&M, is responsible for the development and fabrication of the the trigger.

Hodoscopes—Scintillator, Light Guides, Phototubes and Misc. Supplies: The scintillator and light guide material for the new hodoscopes costs are based on a quote by the Ludlum Corporation. The hodoscope array will need 384 photomultiplier tubes. Of these approximately 160 will be reused from E866 leaving an additional 220 tubes, bases and shields will be recovered from Argonne/HEP's contribution to the Zeus spectrometer at DESY when it is decommissioned in Fall, 2007. The hodoscope arrays are the responsibility of the University

of Illinois and Abilene Christian University (ACU). The collaboration will benefit greatly from the availability of undergraduates students from ACU to work on the hodoscope array.

Tracking For acceptance and rate issues, the E866/NuSea Station 1 tracking chambers will be replaced with new MWPCs. The Station 4 proportional tubes will also be replaced to optimize the acceptance of the spectrometer. The University of Colorado is responsible for the Station 1 tracking chambers, and Los Alamos and Rutgers are responsible for the Station 4 proportional tubes. E906 will benefit greatly by leveraging off of the development work already done at Los Alamos.

Data Acquisition: As mentioned in Sec. 3.9, the E871 DAQ should be sufficient for this experiment [75]. As a contingency, $50k has been allocated for the DAQ.

These costs are also summarized in Tab. IV.

When the experiment was given Phase I approval in 2001, there was a presumption that it would concurrently with other fixed target experiments, and the schedule was allowed to float until the status of those experiment was determined. Rather than wait for a dedicated slow-extraction fixed-target run, E906/Drell-Yan has worked to minimize the instantaneous and integrated impact of the experiment on other proton users by (1) doubling the instantaneous proton rate and thus reducing the number of Main Injector accelerator cycles used and (2) extending the run over two year, thus reducing the instantaneous impact by a factor of two. Combined this reduced the impact by a factor of four, sufficient to allow the experiment to be scheduled. Once this occurred, it was then reasonable to ask DOE/ONP for the funds necessary to upgrade the spectrometer. As mentioned earlier, pending the passage of the Office of Science and the cost and schedule review, E906/Drell-Yan expects to receive funds in early calendar year 2007.

A construction timetable for the new focusing magnet and the upgrade of the spectrometer elements has been developed based on the January 2009 start-of-physics date, but it should be noted that the construction timetable is driven by the availability of funds as much as construction time. The coil design and fabrication, and the assembly of the new magnet are estimated to take 16 months from the beginning of design work (Sept, 2006) through installation of the magnet. Once these operations are completed, two months have been allocated to move the SM3 magnet into position and map its field. The mapping of the new magnet's field will take place during the installation of SM3. The preparation of tracking and hodoscope stations will take place in parallel with magnet construction. After the installation and mapping of the magnets is completed, the

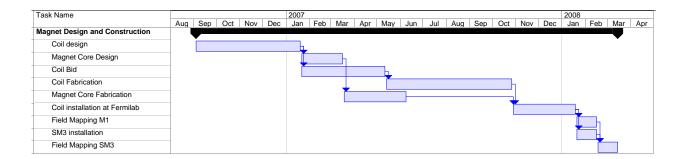| Task Name						2007												2008			
	Aug	Sep	Oct	Nov	Dec	Jan	Feb	Mar	Apr	May	Jun	Jul	Aug	Sep	Oct	Nov	Dec	Jan	Feb	Mar	Apr
Magnet Design and Construction																					
Coil design																					
Magnet Core Design																					
Coil Bid																					
Coil Fabrication																					
Magnet Core Fabrication																					
Coil installation at Fermilab																					
Field Mapping M1																					
SM3 installation																					
Field Mapping SM3																					

FIG. 18: Gantt chart for completion of the E906 spectrometer magnet. The detector construction will be done in parallel with the magnet construction. Much of the detector work can be done elsewhere and installed after the magnets are in place.

more delicate tracking and hodoscope stations will be moved into place in the spectrometer. The magnet construction time-line is shown in Fig. 18.

4.1. Requests of Fermilab

While the collaboration has taken responsibility for most of the spectrometer upgrade, there several items which the collaboration request that Fermilab undertake. These items are listed in appendix B.

5. COLLABORATION FACILITIES AND RESOURCES

The core of the collaboration, Abilene Christian University, Argonne, Fermilab, Los Alamos and Valparaiso University has recently successfully completed the E866 Drell-Yan experiment at Fermilab. These groups encompass the key technologies needed for the new measurements. The Rutgers group has experience in high rate drift chamber systems. The University of Colorado group has built and operated the forward tracking chambers for the HERMES experiment at DESY, which operate in a similar high rate environment. Members of the collaboration have been involved in many previous Drell-Yan and muon pair fixed target experiments at Fermilab including E789, E772 and E605. In addition, we have been contacted by other groups interested in joining this effort.

The design work for the new M1 magnet is being done at Argonne by personnel who formerly worked in the Argonne the ASD division (a part of the Advanced Proton Source). This group has vast experience in designing and realizing magnets for physics experiments. This includes J.M. Jag-

ger, who along with C.N. Brown of Fermilab (also a member of this collaboration) was responsible for the realization of the SM12 magnet which is being replaced by the new M1 magnet [81].

6. CONCLUSIONS

Fermilab E906 will use the 120 GeV primary proton beam from the Main Injector to measure Drell-Yan yields for hydrogen, deuterium and three nuclear targets. These measurements will provide precise new information on:

- the ratio $\bar{d}/\bar{u}$ and the difference $\bar{d} - \bar{u}$ distributions of the proton over the x range of 0.2-0.45 and new insight into the non-perturbative origin of the parton distributions (3.4×10^{18} incident protons),

- the sum $\bar{d} + \bar{u}$ and the high-x valence parton distributions through measurements of the absolute Drell-Yan cross sections

- the nuclear dependence of the antiquark distributions over a similar x range (1.8×10^{18} incident protons), and

- the energy loss of colored partons traveling through cold nuclear matter.

These measurements should also help resolve nuclear ambiguities inherent in obtaining nucleon antiquark distributions from neutrino data on nuclear targets. The total request of 5.2×10^{18} protons can be achieved over two years and an accelerator cycle scheme has been developed to do this, while minimizing the impact on other programmatic uses of protons.

The muon spectrometer needed to carry out this program of measurements is based upon the spectrometers used in previous Fermilab Drell-Yan experiments. Because of the new Superconducting Cryo-Module Test Facility, the experiment has been moved from MEast to the MWest beam line. Much of the equipment from these previous experiments will be reused in the reconfigured spectrometer. Some elements of the spectrometer will need to be replaced for the new experiment. The largest cost associated with this is the construction of a new muon focusing magnet. The funds for these spectrometer upgrades have been requested from DOE/ONP. Subject to the passage of the President's proposed budget for the Office of Science, we have been advised that we can expect funding for these upgrades upon Argonne's completion of a cost and schedule review of this experiment. This will allow for the completion of the spectrometer upgrades and the start of the experiment in January 2009.

APPENDIX A: SUMMARY OF CHANGES OF E906/DRELL-YAN SINCE STAGE I
APPROVAL

There have been a number of changes and developments in the E906/Drell-Yan experiment between the original approval and the present time. All of these have been incorporated into the full document presented to the PAC. This appendix provides a convenient summary of these developments for those already familiar with the experiment.

1. Goals of E906/Drell-Yan

The fundamental physics program of the E906/Drell-Yan experiment has not changed since this experiment was first proposed. The physics is still of fundamental interest and has not been addressed by other measurements. The E906/Drell-Yan measurements will determine $\bar{d}(x)/\bar{u}(x)$ for $0.1 < x < 0.45$. This is accomplished by measuring the ratio of proton-induced Drell-Yan cross sections on hydrogen and deuterium. In addition, the absolute Drell-Yan cross sections are sensitive to the high-x parton distributions of the incoming beam proton. At the same time, the experiment will measure proton-induced Drell-Yan cross sections on a number of nuclear targets. These data will be used to elucidate the nuclear dependence of the sea quark distributions. The entire physics program of E906 is discussed in detail in Sec. 2.

In measuring $\bar{d}(x)/\bar{u}(x)$ the experiment is probing the origin of the partonic sea in the nucleon. The sea was originally believed to arise from gluonic splitting which would produce a flavor symmetric sea [19, 20]. This expectation was not born out in measurements done by the NMC [5] and NA51 [7] collaborations whose results showed $\int \bar{d}(x) - \bar{u}(x)dx = 0.148 \pm 0.039$ and $\frac{\bar{u}}{\bar{d}}\Big|_{x=0.18} = 0.51 \pm 0.04 \pm 0.05$ respectively. Using the Drell-Yan mechanism, Fermilab E866/NuSea measured the ratio of $\bar{d}/\bar{u}$ as a function of x over the range $0.015 \leq x \leq 0.35$ [8, 10]. This data showed a significant excess of $\bar{d}$ quarks over $\bar{u}$ quarks at moderate x, but for $x > 0.25$, the light quark sea started to become symmetric. Unfortunately, this is also the region in which the measurement became statistically limited. E906/Drell-Yan will extend these measurements to larger values of x.

The experiment will also collect Drell-Yan data using nuclear targets. This data will be sensitive to modifications of the sea in nuclei, providing a comparison with νDIS measurements of the strength of the sea. In addition, these data will be a valuable cross check on possible nuclear modifications in the deuterium data which is used to extract $\bar{d}(x)/\bar{u}(x)$. Also of importance is

the information about partonic energy loss which can be extracted from these data. Within the context of different models, analyses of E866/NuSea and E772 nuclear Drell-Yan data show the energy loss of color-charged particles traveling through a colored media is consistent with no energy loss [16] or show significant energy loss [66]. The data collected by E906/Drell-Yan will be able to clearly distinguish between these models. A brief but interesting discussion of partonic energy loss measurements may be found in Ref. [67]

2. Other Proposed Measurements of the Sea Quark Flavor Asymmetry

There are no significant competing measurements of the flavor dependence of the antiquark distributions of the proton or of the nuclear dependence of the sea quarks. Experiments using semi-inclusive deep inelastic scattering (SIDIS) at Jefferson Laboratory (JLab) and a similar Drell-Yan experiment at JPARC have both been recently been considered by the PACs at the respective laboratories. While the physics goals were considered interesting, both proposals were deferred. Additional discussion of these measurements can be found in Sec. 2.1.3.

Semi-Inclusive Deep Inelastic Scattering (SIDIS) was used by the HERMES collaboration [36] to extract $\bar{d}(x) - \bar{u}(x)$. The results agree well with the E866/NuSea measurement, but with significantly larger statistical uncertainties. An experiment was proposed to the Jefferson Laboratory (JLab) PAC for the future 12 GeV facility to repeat these measurement with an 11 GeV electron beam in JLab Hall C [38]. The JLab PAC deferred this proposal. Even if approved as proposed, this SIDIS experiment covered a more limited range in x and lacked statistical sensitivity (measurements on the order of 10-15%, to be compared with 1-4% for most of the E906/Drell-Yan data). In addition, there were significant systematic uncertainties in extracting $\bar{d}(x) - \bar{u}(x)$ from the SIDIS measurements.

A Drell-Yan measurement of $\bar{d}(x)/\bar{u}(x)$, in contrast, has relatively small systematic uncertainties. At JPARC, a Drell-Yan proposal was submitted in Spring, 2006, to measure $\bar{d}(x)/\bar{u}(x)$ [82] using a 50 GeV proton beam. The initial Phase I, the JPARC facility will be able to provide up to 30 GeV proton beams, but there are plans for an eventual upgrade to at 50 GeV beam. With just 30 GeV, the available mass region is severely limited, and the di-muon program of this experiment would be limited to J/ψ studies, and the Drell-Yan thrust of the experiment would necessarily have to wait until the 50 GeV beam would be available. The JPARC recognized the importance of these measurements but deferred the experiment, citing the uncertainty of the time line for achieving a

50 GeV beam line. Other difficulties in the implementation of the E906/Drell-Yan physics program with a 50 GeV beam are discussed in Sec. 2.1.3.

To measure the flavor asymmetry of the nucleon sea and/or the nuclear dependence of the sea, Drell-Yan scattering is still clearly the best method. Fermilab E906/Drell-Yan is the the only experiment that is posed to make these measurements.

3. Experimental Schedule, Beam Structure

E906/Drell-Yan was granted Phase I approval in 2001. At that time, there was a presumption, because of proton economics[7], that it would be part of a future, but unscheduled, fixed target run which would include a number of other experiments such as the proposed CKM and KAMI experiments. In 2004, when it became clear that a major fixed target run would not take place in the near future, an alternative run strategy was discussed which enabled E906/Drell-Yan to be placed on a tentative schedule.

In order to do this, the instantaneous impact of the E906 on other proton users was cut by a factor of approximately four. First, length of the run was doubled from one to two years, reducing the number of MI cycles needed per year by two. Secondly, the experiment will is now planning on taking 2×10^{12} protons/s rather than the proposed 1×10^{12} protons/s. This is twice the originally proposed instantaneous luminosity, providing another factor of two reduction in the amount of MI time needed to deliver the requested 5.2×10^{18} protons[8]. The experience with rate dependent effects from e866/NuSea [83] lead us to believe that systematic uncertainties due to target related rate effects can still be easily understood and modeled with these rates.

One possible scenario for implementing this, discussed by the Meson Beam Task Force would be to have a 5 s slow extraction spill every minute with a total of 1×10^{13} protons. The proposed scheme will diminish protons available to other uses by 13%. This scheme also allows E907/MIPP and the test beam facility to be run with no additional impact.

---

[7] In fact, the number of protons needed by the experiment is relatively small, but the opportunity cost of the lost cycles could have effected antiproton production.

[8] The Meson Beam Task Force rounded this request up to 6.0×10^{18} for planning purposes

4. Experimental Location

The experiment as proposed in 1999 and 2001 was to take place in the Meson East (MEast) experimental area where E772, E789 and E866 had run. This had the advantage that much of the infrastructure, including the beam line, suitable foundations for both dipole magnets were already in place. In 2005, however, an effort was begun to transform this area into a Superconducting Cryo-Module Test Facility. E906 was tentatively moved to the MWest beam-line. While not the ideal location for E906 (it is rather cramped as compared with the previous location in MEast) there is sufficient room for the spectrometer and it will work. There is clearly some additional cost to Fermilab because of this move, which was presumably balanced against the need for to place the Superconducting Cryo-Module Text Facility in MEast. The recommissioning of this beam line and the location of the experiment is the subject of a recently completed Meson Beam Task Force study chaired by Dave Christian [71].

5. Second Dipole: SM3 instead of the Jolly Green Giant

As originally proposed, E906/Drell-Yan was to used the Jolly Green Giant (JGG) as the second dipole magnet of the spectrometer. The central function of this magnet is to measure muon momentum. Previous Drell-Yan experiments (E772, E866, etc) had used the SM-12 dipole with an aperture of 60×60 inches and field integral of 3 T-m. This magnet is much better suited that the JGG (which has an aperture of 80×50 inches and a field integral of 1.65 T-m) for the E906/Drell-Yan experiment. There is a slight acceptance cost since SM3 is significantly longer, causing the downstream tracking station to be positioned further from the target and thus reducing its angular coverage in x slightly. When E906 was proposed, however, it was not available. It is now available and we have made arrangements to used this magnet instead. This change will also free up the JGG for continued use in other experimental programs, including E907.

6. Trigger

In the original proposal, the trigger was to be based on LeCroy 2367 Logic modules. These were highly programmable units that would allow the experiment to "track" roads through the detector based on hodoscope hit patterns. Since this measurement was originally proposed, LeCroy has ceased to make these modules. Fortunately, in the mean time the cost and complexity of using

FPGA (Field Programmable Gate Arrays) have decreased significantly. The collaboration now plans to implement nearly identical trigger logic in FPGA's. The full logic of the trigger scheme is described in Sec. 3.6.

7. DOE/ONP Funding for the Spectrometer

Most of the funds to construct the new coils for the first dipole and to update the detectors will come from DOE, Office of Nuclear Physics. There is a *minimum* of a two year lead time to be placed into the DOE Office of Nuclear Physics funding cycle and this could not happen until the experiment was actually scheduled by Fermilab. DOE Office of Nuclear Physics has asked Argonne to hold a review of the cost, schedule and risks involved with the construction of the new magnet and upgrade of the spectrometer. This review will be completed this fall. Assuming a positive review, we have been advised that with Office of Science Budgets close to the President's proposed budget we can expect Office of Nuclear Physics funding to begin shortly after the Federal budget is passed. Design work on the coils has already begun and it is anticipated that a request for bids from vendors will be made in Spring 2007. (See Sec. 4 for more details.)

APPENDIX B: REQUESTS FOR FERMILAB

In planning for the experiment and the spectrometer upgrade, most of the tasks directly related to the spectrometer upgrade have been take on by the collaboration. There are some areas, however, for which we are specifically requesting that Fermilab take responsibility. These are itemized below.

- Provide slow extracted beam of 120 GeV proton at a rate of no more than $2/time10^{12}$/s for a total of 5.2×10^{18} protons on target in two years.

- Provide beam line and instrumentation.

- Assemble New M1 magnet in MWest area from coils and pole tips supplied by Argonne and return yoke from SM12. This includes providing a suitable foundation for the magnet now that the experiment has been moved to MWest.

- Provide and install beam dump in M1 magnet with necessary water cooling. The E866/NuSea beam dump should be able to be modified for this.

- Modify SM12 flux return steel as necessary for new magnet. This specifically includes cutting the steel blocks on the top and bottom of the magnet since the new magnet is narrower than SM12.

- Install SM3 in MWest. Again, This includes providing a suitable foundation for the magnet now that the experiment has been moved to MWest.

- Provide magnet power supplies.

- Provide utilities (power and cooling water) for magnets and power supplies.

- Install muon ID absorber walls using material from E866/NuSea.

- Provide liquid hydrogen and deuterium targets and drive mechanism to interchange solid and liquid targets remotely. If the E866/NuSea targets and drive mechanism are still available, these would also work for E906/Drell-Yan.

- Provide PREP electronics for the experiment. Specifically, this consists of the E866 PREP electronics plus 1700 channels of multi-hit TDC (LeCroy 3377) and 32 channels of mean timers.

- Provide chamber gas distribution system plumbing

- Provide flammable gas safety system.

- Provide appropriate radiation shielding, radiation safety interlocks and handle all aspects of radiation safety monitoring.

- Provide rigging for installation.

- Provide counting house and electronics areas with appropriate utilities and networks installed.

- Provide facilities for scintillator and light guide fabrication.

- Provide equipment staging areas as needed for the assembly of the spectrometer.

- Provide two analysis workstations for counting house.

[1] J. Pumplin et al., JHEP **07**, 012 (2002), hep-ph/0201195.

[2] A. D. Martin, R. G. Roberts, W. J. Stirling, and R. S. Thorne, Eur. Phys. J. **C28**, 455 (2003), hep-ph/0211080.

[3] A. D. Martin, R. G. Roberts, W. J. Stirling, and R. S. Thorne, Eur. Phys. J. **C35**, 325 (2004), hep-ph/0308087.

[4] M. Gluck, E. Reya, and A. Vogt, Eur. Phys. J. **C5**, 461 (1998), hep-ph/9806404.

[5] P. Amaudruz et al. (New Muon), Phys. Rev. Lett. **66**, 2712 (1991).

[6] M. Arneodo et al. (New Muon), Phys. Rev. **D50**, 1 (1994).

[7] A. Baldit et al. (NA51), Phys. Lett. **B332**, 244 (1994).

[8] E. A. Hawker et al. (FNAL E866/NuSea), Phys. Rev. Lett. **80**, 3715 (1998), hep-ex/9803011.

[9] J. C. Peng et al. (E866/NuSea), Phys. Rev. **D58**, 092004 (1998), hep-ph/9804288.

[10] R. S. Towell et al. (FNAL E866/NuSea), Phys. Rev. **D64**, 052002 (2001), hep-ex/0103030.

[11] H. L. Lai et al. (CTEQ), Eur. Phys. J. **C12**, 375 (2000), hep-ph/9903282.

[12] A. D. Martin, R. G. Roberts, W. J. Stirling, and R. S. Thorne, Eur. Phys. J. **C39**, 155 (2005), hep-ph/0411040.

[13] H. L. Lai et al., Phys. Rev. **D55**, 1280 (1997), hep-ph/9606399.

[14] A. D. Martin, R. G. Roberts, and W. J. Stirling, Phys. Lett. **B387**, 419 (1996), hep-ph/9606345.

[15] D. F. Geesaman, K. Saito, and A. W. Thomas, Ann. Rev. Nucl. Part. Sci. **45**, 337 (1995).

[16] M. A. Vasilev et al. (FNAL E866), Phys. Rev. Lett. **83**, 2304 (1999), hep-ex/9906010.

[17] A. D. Martin, W. J. Stirling, and R. G. Roberts, Phys. Lett. **B252**, 653 (1990).

[18] R. D. Field and R. P. Feynman, Phys. Rev. **D15**, 2590 (1977).

[19] D. A. Ross and C. T. Sachrajda, Nucl. Phys. **B149**, 497 (1979).

[20] F. M. Steffens and A. W. Thomas, Phys. Rev. **C55**, 900 (1997), nucl-th/9612056.

[21] W. Melnitchouk, J. Speth, and A. W. Thomas, Phys. Rev. **D59**, 014033 (1999), hep-ph/9806255.

[22] A. Szczurek, M. Ericson, H. Holtmann, and J. Speth, Nucl. Phys. **A596**, 397 (1996), hep-ph/9602213.

[23] P. V. Pobylitsa, M. V. Polyakov, K. Goeke, T. Watabe, and C. Weiss, Phys. Rev. **D59**, 034024 (1999), hep-ph/9804436.

[24] A. E. Dorokhov and N. I. Kochelev, Phys. Lett. **B304**, 167 (1993).

[25] P. Geiger and N. Isgur, Phys. Rev. **D55**, 299 (1997), hep-ph/9610445.

[26] S. Kumano, Phys. Rev. **D43**, 59 (1991).

[27] S. Kumano, Phys. Rev. **D43**, 3067 (1991).

[28] G. 't Hooft, Phys. Rev. **D14**, 3432 (1976).

[29] A. D. Martin, R. G. Roberts, W. J. Stirling, and R. S. Thorne, Eur. Phys. J. **C23**, 73 (2002), hep-ph/0110215.

[30] G. T. Bodwin, Phys. Rev. D **31**, 2616 (1985).

[31] G. T. Bodwin, Phys. Rev. D **34**, 3932 (1986).

[32] G. T. Bodwin, S. J. Brodsky, and G. P. Lepage, Phys. Rev. **D39**, 3287 (1989).

[33] W. G. Seligman et al., Phys. Rev. Lett. **79**, 1213 (1997).

[34] U.-K. Yang et al. (CCFR/NuTeV), Phys. Rev. Lett. **86**, 2742 (2001), hep-ex/0009041.

[35] M. Vakili et al. (CCFR), Phys. Rev. **D61**, 052003 (2000), hep-ex/9905052.

[36] K. Ackerstaff et al. (HERMES), Phys. Rev. Lett. **81**, 5519 (1998), hep-ex/9807013.

[37] X. Jiang et al. (2002), JLlab PR-02-107.

[38] A. Bruell, H. Gao, H. Mkrtchyan, et al. (2006), JLab PR12-06-111.

[39] D. M. Alde, H. W. Baer, T. A. Carey, G. T. Garvey, A. Klein, C. Lee, M. J. Leitch, J. W. Lillberg, P. L. McGaughey, C. S. Mishra, et al., Phys. Rev. Lett. **64**, 2479 (1990).

[40] J. Stirling (1998), letter ot John Peoples.

[41] G. Moreno et al., Phys. Rev. **D43**, 2815 (1991).

[42] W. Melnitchouk and A. W. Thomas, Phys. Lett. **B377**, 11 (1996), nucl-th/9602038.

[43] S. Kuhlmann et al., Phys. Lett. **B476**, 291 (2000), hep-ph/9912283.

[44] J. C. Webb, Ph.D. thesis, New Mexico State University (2003), hep-ex/0301031.

[45] J. J. Aubert et al. (European Muon), Phys. Lett. **B123**, 275 (1983).

[46] S. A. Kulagin and R. Petti, Nucl. Phys. **A765**, 126 (2006), hep-ph/0412425.

[47] J. Carlson and R. Schiavilla, Rev. Mod. Phys. **70**, 743 (1998).

[48] E. L. Berger, F. Coester, and R. B. Wiringa, Phys. Rev. **D29**, 398 (1984).

[49] E. L. Berger and F. Coester, Phys. Rev. **D32**, 1071 (1985).

[50] F. Coester (2001), private communication.

[51] H. Jung and G. A. Miller, Phys. Rev. **C41**, 659 (1990).

[52] G. E. Brown, M. Buballa, Z. B. Li, and J. Wambach, Nucl. Phys. **A593**, 295 (1995), nucl-th/9410049.

[53] A. E. L. Dieperink and C. L. Korpa, Phys. Rev. **C55**, 2665 (1997), nucl-th/9703025.

[54] J. R. Smith and G. A. Miller, Phys. Rev. Lett. **91**, 212301 (2003), nucl-th/0308048.

[55] K. Adcox et al. (PHENIX), Phys. Rev. Lett. **88**, 022301 (2002), nucl-ex/0109003.

[56] C. Adler et al. (STAR), Phys. Rev. Lett. **89**, 202301 (2002), nucl-ex/0206011.

[57] K. Adcox et al. (PHENIX), Phys. Lett. **B561**, 82 (2003), nucl-ex/0207009.

[58] C. Adler et al. (STAR), Phys. Rev. Lett. **90**, 032301 (2003), nucl-ex/0206006.

[59] C. Adler et al. (STAR), Phys. Rev. Lett. **90**, 082302 (2003), nucl-ex/0210033.

[60] S. Gavin and J. Milana, Phys. Rev. Lett. **68**, 1834 (1992).

[61] S. J. Brodsky and P. Hoyer, Phys. Lett. **B298**, 165 (1993), hep-ph/9210262.

[62] R. Baier, Y. L. Dokshitzer, A. H. Mueller, S. Peigne, and D. Schiff, Nucl. Phys. **B484**, 265 (1997), hep-ph/9608322.

[63] R. Baier, Y. L. Dokshitzer, A. H. Mueller, and D. Schiff, Nucl. Phys. **B531**, 403 (1998), hep-ph/9804212.

[64] K. J. Eskola, V. J. Kolhinen, and C. A. Salgado, Eur. Phys. J. **C9**, 61 (1999), hep-ph/9807297.

[65] K. J. Eskola, V. J. Kolhinen, and P. V. Ruuskanen, Nucl. Phys. **B535**, 351 (1998), hep-ph/9802350.

[66] M. B. Johnson et al., Phys. Rev. **C65**, 025203 (2002), hep-ph/0105195.

[67] G. T. Garvey and J. C. Peng, Phys. Rev. Lett. **90**, 092302 (2003), hep-ph/0208145.

[68] F. Arleo, Phys. Lett. **B532**, 231 (2002), hep-ph/0201066.

[69] E. Wang and X.-N. Wang, Phys. Rev. Lett. **89**, 162301 (2002), hep-ph/0202105.

[70] M. Hirai, S. Kumano, and M. Miyama, Phys. Rev. **D64**, 034003 (2001), hep-ph/0103208.

[71] D. Christian et al., *Report of the "Meson Beam Task Force"* (2006).

[72] A. Walters (2001), private Communication.

[73] C. A. Gagliardi et al., Nucl. Instrum. Meth. **A418**, 322 (1998).

[74] D. Geesaman et al. (E906/Drell-Yan) (1999), unpublished.

[75] Y.-C. Chen (2001), private communication.

[76] R. Pordes et al., in *Computing in High Energy Physics (CHEP 94)* (San Francisco, CA, 1994), http://fnalpubs.fnal.gov/archive/1994/conf/Conf-94-103.pdf.

[77] J. Jagger and K. Thompson (2002), unpublished.

[78] SigmaPhi (2005), private communication/Budgetary Estimate.

[79] E. Tesla (2005), private communication/Budgetary Estimate.

[80] Stangenes (2005), private communication/Budgetary Estimate.

[81] R. Fast, E. Bosworth, C. Brown, D. Finley, A. Glowacki, J. Jagger, and S. Sobczynski (1981), fermilab report TM-1034.

[82] J.-C. Peng, S. Sawada, et al. (2006).

[83] R. S. Towell, Ph.D. thesis, University of Texas (2001), nucl-ex/0102012.